Acta virologica **62**: 310 – 325, 2018 doi:10.4149/av_2018_225

Time-course of transcriptome response to respiratory syncytial virus infection in lung epithelium cells

S. AMPUERO[1], R. ANDAUR[1], M. MILANO[1], M. MORENO[2], L. LIZAMA[1], C. LARRAÑAGA[1], U. URZÚA[3]

[1]Virology Program, Institute of Biomedical Sciences, Faculty of Medicine, University of Chile; Postal address 8380453, Independencia 1027, Independencia, Santiago, Chile; [2]Laboratory of Oncology and Molecular Genetics, Coloproctology Unit, Clinica Las Condes, Santiago, Chile; Postal address 7591046, Santiago, Chile; [3]Department of Basic and Clinical Oncology, Faculty of Medicine, University of Chile, Postal adress 8380453, Santiago, Chile

Received December 27, 2017; revised February 2, 2018; accepted July 12, 2018

Summary. – Respiratory syncytial virus (RSV) is the major cause of acute lower respiratory tract infection in infants. Winter outbreaks in Chile result in 5% of infected children hospitalized, with 0.01% mortality. Increased evidence indicates that viral and host factors modulate the severity of infection. Using DNA microarrays, we characterized the genome-wide transcriptional response of lung mucoepidermoid cells (NCI-H292) at 0, 24, 48, 72 and 96 hours post-infection (hpi) with a single dose of RSV/A. During the whole studied period, a bi-phasic gene expression profile was observed by a total of 330 differentially expressed genes. About 60% of them were up-regulated between 24–72 hpi and then turned-off at 96 hpi. This transient, early gene expression pattern was significantly enriched in biological processes like interferon signaling, antigen processing and presentation, double-stranded RNA binding and chemokine activity. We detected 27 common genes up-regulated between 24–72 hpi, from which IFIT1, IFI44, MX1, CXCL11 and OAS1 had the highest expression. The second pattern comprised over 120 genes, which remained silenced until 72 hpi, but were steeply up-regulated by 96 hpi. Biological processes of this late-response profile included cell cycle division and microtubule cytoskeleton organization. Conversely, the genes belonging to virus response pathway showed a decreased expression at 96 hpi. We conclude that RSV induces an early innate immune activation profile response until 72 hpi. Thereafter, the viral response is inhibited, leading to host cell recovery. The presented cellular model allows to study the specific pathways involved in elimination of infection at prolonged time intervals and their subsequent analysis in severe RSV disease of infants and/or older adults.

Keywords: RSV; NCI-H292 cells; microarrays; time-course; gene expression profile

Introduction

Respiratory syncytial virus (RSV) is recognized as the main respiratory pathogen causing illness in children, presenting a higher morbidity in infants younger than 6 months and also in elderly population. RSV causes illness ranging from a mild upper respiratory tract to severe lower respiratory tract illness (LRTI), with bronchiolitis being its main clinical manifestation (Tregoning and Schwarze, 2010; Griffiths *et al*., 2017). Studies performed in our country showed that previously healthy term infants younger than 6 months of age hospitalized due to LRTI-RSV, developed varied clinical outcome severity, while 50% showed a severe outcome and 21% or less presented low severity outcome after hospitalization (Luchsinger *et al*., 2014). Different factors have been postulated to explain these differences, depending on the virus, the viral load, circulating genotypes and the host as immune response and genetic susceptibility (Ampuero *et al*., 2011; Luchsinger *et al*., 2014; Rusell *et al*., 2017).

E-mail: sampuero@u.uchile.cl; phone: +56-2-29786961.

Abbreviations: HCL = hierarchical clustering; hpi = hour(s) post-infection; IFA = indirect immunofluoresce assay; Fc = fold change; LTRI = lower respiratory tract illness; RSV = respiratory syncytial virus; SSC = saline sodium citrate buffer

RSV belongs to the family *Paramyxoviridae*, the genus *Pneumovirus*. It is an enveloped virus; its genome consists of a linear, non-segmented negative single-strand RNA (ssRNA), which encodes for 10 subgenomic mRNAs and 11proteins: NS1, NS2, N, P, M, SH, F, G, M2-1, M2-2, L. Infection occurs by direct contact with aerosol containing viral particles. RSV replicates in the nasopharynx, its incubation period lasts 4–5 days and viral excretion can be detected between 1–21 days. RSV propagates down to the lower respiratory tract in just 1–3 days. The virus disseminates from cell to cell without contacting the extracellular medium and forms syncytia, a known RSV cytopathic effect (Collins *et al*., 2013). The direct replication of RSV would not be implied in the disease onset, as histopathological and *in vitro* models show rather the inflammatory mediators of immune response to be associated with RSV pathogenesis and disease development (Welliver *et al*., 2008; Collins and Melero, 2011; Rusell *et al*., 2017). After infection, the RSV-infected cells detect viral components, especially viral RNA and intermediates of virus replication, through receptors as the Toll-like receptors (TLRs), retinoic acid-inducible gene-I-(RIG-I-) like receptors (RLRs), and nucleotide-binding oligomerization domain-(NOD-) like receptors (NLRs) (Gouba *et al*., 2013; Kim and Lee, 2014). Activation of these receptors triggers a signaling pathway that allows activation of gene expression of pro-inflammatory cytokines and chemokines and interferon α and β (Mukherjee and Lukacs, 2013). In turn, the response to interferon modulates the activation of interferon-stimulated genes (ISGs) (Takaoka and Yanai, 2006). Altogether, all these immune response signals allow the triggering of antiviral response at the cellular level and systemically attract immune cells to the infection site while activating the acquired immune response. On the other hand, the virus itself is able to modulate this response. It has been established that RSV proteins NS1 and NS2 interfere with the activation of ISGs, suppress dendritic cell maturation and cytokines production (Barik, 2013; Schmidt and Varga, 2017). Nowadays, there are no effective antivirals or anti-RSV vaccines that have a real impact on diminishing the number of infected subjects or an attenuation of the severity of the disease caused by RSV. Only Palivizumab, a humanized monoclonal antibody, is recommended for prophylaxis in infants at high-risk to develop severe RSV disease (Turner *et al.*, 2014).

In spite of multiple studies regarding RSV infection, some aspects of RSV-host interaction are still unclear. Changes in gene expression after RSV infection using microarray platforms have delivered a great amount of information of pathways and molecules involved during the infection. Moreover, the use of cell lines susceptible to RSV infection, although far from the global response of the individual, allows designing controlled studies and to specifically focus on cell and molecular pathways (Zhang *et al*., 2001; Fjaerli *et al*., 2006; Janssen *et al*., 2007; Martínez *et al*., 2007; Mayer *et al*., 2007; Huang *et al*., 2008; Mejías *et al*., 2013). Several studies have analyzed the gene expression profile after RSV infection in cell models at early times after infection. However, the majority of symptomatic cases consult after 2 to 3 days of the onset of symptoms, for this reason the establishment of *in vitro* models that cover the time-course of RSV infection could contribute to better understanding of the pathogenesis of this virus. In addition, considering that infants with an RSV infection without known risk factors can develop conditions of variable severity, expression studies in this specific population would indicate the pathways that could be studied more specifically using a suitable cellular model. Our aim was to analyze variations in gene expression of a pulmonary epithelial cell line, NCI-H292, infected with RSV/A at different times after infection using Human Exonic Evidence Based Oligonucleotide (HEEBO) array.

Materials and Methods

Cells and culture conditions. The human lung epithelial cell line NCI-H292 was purchased from the American Type Culture Collection (CRL-1848, MD, USA) and grown at 37°C in 5% CO_2 in RPMI-1640 medium (HyClone) supplemented with 10% FBS, 100 U/ml penicillin, 100 µg/ml streptomycin, 10 mmol/l HEPES free acid and 1x MEM-non essential aminoacids solution.

*Preparation of the RSV inoculum.*RSV/A/Tracy (Luchsinger *et al*., 2012) was propagated in MA104 cells as previously described (Chen *et al*., 2002).Virus stocks were obtained within 3 days after infection and then stored in 1 ml aliquots at -80°C. For plaque titration of RSV aliquots, 70% confluent NCI-H292 cells were grown in 6-well plates with RPMI-1640 2X supplemented with2% FBS. Then 0.5 ml serial dilutions of virus stocks were added and incubated at 37°C. After 1 h, 2.5 ml of 1.2% agarose was added to each well and the plates were incubated at 37°C in CO_2 incubator for 7 days. The plaques were visualized and counted using methyl violet staining.

RSV infection, cell harvesting and RNA extraction. NCI-H292 cells grown to 70% confluence were treated with a 1x PBS, 50 mmol/l EDTA pH 8.0 solution for 10 min at 37°C to release them from culture flask surface. Cell suspension was centrifuged at 800 x g for 10 min. The resulting cell pellet, 5 x 10^6 cells, was resuspended in 2 ml of RPMI-1640 medium and infected with 4.8 x 10^5 PFU of RSV-A strain (approximately 5 log PFU/ml), getting a MOI of 0.1. Cultures were incubated at 37°C in 5% CO_2 and cells were harvested at 0, 24, 48, 72 and 96 hours post-infection (hpi). Control, uninfected cultures were set-up simultaneously and cells collected at the indicated times. Total RNA was extracted with Trizol (GIBCO BRL Life Technologies), treated with RNase-free DNase (QIAGEN) and cleaned up with the RNeasy Mini Kit (QIAGEN). RNA integrity was assessed by measuring the 28S/18S ratio in 1%

agarose gels. RNA concentration was determined by A_{260} /A_{280} nm spectrophotometry (Epoch, Biotek Instruments).

RSV detection. Confirmatory indirect immunofluorescence assay (IFA) for RSV infection was performed in cell cultures as described using monoclonal antibodies, 133-1H and 92-11C, that react with the fusion protein (F), (kindly provided by L. Anderson, Centers for Disease Control and Prevention, Atlanta, Georgia) (Avendaño *et al*., 2003). Total RNA was extracted from supernatant of infected cell cultures. Qualitative detection of RSV was done with real-time reverse transcription polymerase chain reaction (real time RT-PCR) as described previously (Luchsinger *et al*., 2014).

cDNA labeling and microarray hybridization. Equal amounts of RNA isolated from infected and uninfected cultures were fluorescence labeled in parallel. Namely, 15 μg of DNAse-treated purified RNA samples were tagged either with Cy3-dUTP (GE Healthcare) or Cy5-dUTP (GE Healthcare) by reverse transcription using Superscript II Reverse Transcriptase (Invitrogen). Dye swap was conducted for each sample pair analyzed. Labeled cDNAs were mixed and cleaned up with Mini Elute PCR columns (QIAGEN). Purified cDNA mixture was combined with an equal volume of hybridization solution (1x SSC, 50% deionized formamide, 0.1% SDS and 20 μg of salmon sperm DNA), incubated at 95°C for 3 min and then at 37°C for 5 min. This solution was deposited onto HEEBO microarrays (MI, Microarrays.Inc), covered with LifterSlip coverslips and incubated at 42°C for 18 h in Telechem hybridization cassettes. Then, microarray slides were washed with solutions of decreasing salt concentration (2x SSC plus 0.1% SDS; 1x SSC; 0.2x SSC), dried and immediately scanned in a ScanArray Lite (PelkinElmer) set at 90% of laser power and 60–70% of PMT gain. TIFF microarray images were analyzed with the GenePixPro6.0software (Molecular Devices).

Data processing, statistical and functional analysis. GPR files and composite microarray images were deposited to the NCI`s microarray database (mAdb; http://madb.nci.nih.gov/). Microarray data was intra and inter-slide normalized by the local print-tip Loess method with background subtraction using the DNMAD tool (http://asterias.bioinfo.cnio.es). An ANOVA test with false discovery rate (FDR) control was performed with the tool Pomelo II (http://pomelo2.bioinfo.cnio.es). The time course analysis and hierarchical clustering (HCL) were performed with TMEV tool v4.7 using average linkage and leaf order optimization as linkage method and Euclidean distance as distance metric. Differentially expressed genes ($p < 0.01$) in response to viral infection were filtered out with $\log_2$ fold-change (Fc): ≥1.0 or ≤-1.0 for further biological significance analysis. Statistically significant gene ontology (GO) categories were obtained after the functional enrichment analysis using the WebGestalt online tool (www.webgestalt.org) with hypergeometric algorithm and Benjamini-Hochberg multiple testing correction. The common genes at different hpi were determined with Venn diagrams (http://bioinformatics.psb.ugent.be/webtools/Venn).

Relative quantification of selected genes by real time RT-PCR. A real time RT-PCR assay based on SYBR-Green detection was used to confirm the relative gene expression of a selected set of genes. Total RNA was obtained for each viral infection as previously described, treated with RNase-free DNase (QIAGEN) and quantified by measuring absorbance at 260 nm (Epoch, Biotek Instruments). The cDNAs were obtained from 1 μg RNA using M-MLV Reverse Transcriptase (Promega) and random primers (Promega) according to the manufacturer's guidelines. Real time RT-PCR was performed using specific primers designed from NCBI sequences and the software Beacon Designer 8.02 (PREMIER Biosoft). The

Table 1. Forward and reverse gene-specific primers and thermal cycling conditions for real time RT-PCR

Gene symbol	GenBank Acc. No.	Forward (F) and reverse (R) primers	Thermal cycling conditions*
B2M	NM_004048.2	F: TGTAAGCAGCATCATGGA	95°C x 3 s
		R: AGTGTAAGTGTATAAGCATATCAA	53°C x 20 s
HLA-A	NM_002116.2	F: GAGATGGGAGCTGTCTTC	95°C x 3 s
		R: CTCTTCCTCCTCCACATC	60°C x 10 s
HPRT1	NM_00194.2	F: GGTCAGGCAGTATAATCCA	95°C x 3 s
		R: GCTTATATCCACACTTCGT	58°C x 20 s
IFI44	NM_006417.2	F: TCTGAGACGAATGCTATG	95°C x 3 s
		R: CTTCTGTGATGTGAGGAA	59°C x 15 s
			72°C x 10 s
IRF9	NM_006984.2	F: TGATACAGCTAAGACCAT	95°C x 3 s
		R: CTCCTTATACTTTCCCTTAA	56°C x 20 s
			72°C x 15 s
STAT1	NM_007315.2	F: TATATCAAGACTGAGTTG	95°C x 5 s
		R: CTATACTGTGTTCATCAT	54°C x 20 s
			72°C x 20 s
STAT2	NM_0019833.2	F: ACCAAGGACCTGTATCAC	95°C x 3 s
		R: TTCTTCAATCTTTACACAGTTTC	60°C x 5 s

*Initial activation step was at 95°C for 3 min. All reactions were run with 45 cycles.

sequences of the primers are shown in Table 1. The PCR reaction was performed using the KAPA SYBR© Fast qPCR (Kapa Biosystems) with 1 µl of cDNA in a final volume of 10 µl according to the Eco™ Real-Time PCR system (Illumina) protocol. The efficiency of each real-time RT-PCR assay was determined before the sample amplification. Final reaction settings are shown in Table 1. Gene expression fold changes were determined using the $2^{-\Delta\Delta CT}$ method with HPTR1 as housekeeping gene for normalization (Livak and Schmittgen, 2001). Data were analyzed by one-way analysis of variance (ANOVA) using Sigma Stat 3.5® (Systat Software Inc) and GraphPad Prism 7.0® (GraphPad Software, Inc).

Results

RSV infection

NCI-H292 cells were inoculated with RSV (MOI 0.1) and maintained until 96 h. The cells showed cytological alterations and distribution changes, forming clusters as early as 24 h after RSV infection. Such changes remained by 72 and 96 hpi. At 96 hpi, cell clusters comprised a higher cell number in respect to earlier infection times. However, we did not observe syncytia under these conditions. Viral replication was verified at 96 hpi by detecting viral proteins using IFA and the presence of viral genome by real time RT-PCR.

Genes differentially expressed during RSV infection

To determine changes in gene expression after RSV infection (approximately 5 log PFU/ml; MOI: 0.1) of NCI-H292 cells during prolonged times, the HEEBO microarray was used. Then, total RNA was isolated at 24, 48, 72 and 96 hpi and the corresponding labeled cDNA hybridized to HEEBO arrays. RNA at time 0 was also obtained. Microarray hybridization images extracted and normalized as described in Material and Methods, resulted in a global list of 16,487 probes with detectable fluorescent intensity ratios for the four time points analyzed including dye-swap replicates. The global list was subjected to an ANOVA limma test resulting in 533 significant probes ($p < 0.01$) across all time points analyzed. For further analyses, for the probes that detected the same gene an average intensity per hour post-infection was calculated and only one identifier per gene was included, moreover, any repeats, unmapped ESTs and virus coding were excluded, giving rise to an end list constituted by 339 unique genes.

We performed the hierarchical clustering analysis (HCL) using the 339 differentially expressed genes at four post infection time points, including the profile obtained at time 0 (Fig. 1a). A bi-phasic gene expression profile was observed during the whole studied period. About 60% of genes were up-regulated between 24–72 hpi and then turned-off at 96 hpi. A profile of 208 down-regulated genes and 131 up-regulated genes was obtained at 96 hpi as is shown in Fig. 1a. We eliminated nine designed probes with "orf" or non-protein coding RNA. The Supplementary Table S1 shows genes and fold change (Fc) at each time. Considering only the genes whose fold change, expressed as Fc, was between ≥ 1 and ≤ -1 at each hpi, we observed the same profile as in HCL, there are mostly more up-regulated genes at 24, 48 and 72 hpi (Fig. 1b). The range of intensity was selected to analyze more relevant changes in mRNA levels. At time 0 no genes were included in the previous range. All further analyses were performed only with genes meeting that criterion of intensity (≥ 1 and ≤ -1).

Changes in gene expression at different post infection times

Common up-regulated genes and GO enrichment analysis

Overlapping up-regulated genes at each post-infection time were analyzed by Venn Diagram. Among the 330 differentially expressed genes, we did not detect common up-regulated genes when the four post-infection times were compared. However, 27 common genes were up-regulated when 24, 48 and 72 hpi were contrasted (Venn Diagram, Fig. 1c). In Table 2 are listed these 27 genes and their fold changes according to each post-infection time and considering the 24 hpi time to order Fc values from highest to lowest. Among them, IFIT1, IFI44, MX1, CXCL11 and OAS1 are the genes that presented the highest expression at earlier post infection times (Fc>3) and this same group had a diminished expression at 96 hpi.

The cell response against RSV triggers intracellular signaling as well as extracellular pathways to activate an antiviral state (Rusell *et al.*, 2017). Many of the pathways of innate immune response are activated early as we also observed with the group of common up-regulated genes. Through the GO enrichment analysis, we detected four biological processes with seven or more genes belonging to each pathway, in which these 27 genes are involved, as described in Table 3. Of these common genes 51.8% (14/27) belonged to pathways of response to interferon (IFN) α and β. Together with these pathways, we identified that many genes that are up-regulated participate in the processes of antigen processing and presentation of exogenous peptide antigen. The activation of these four pathways during the first three days after infection suggested that this cell type responds rapidly to infection and triggers the immune response to terminate the infection. This sort of response was also found when analyzing the molecular functions, in which these genes participate. Among the detected molecular functions, two presented higher enrichment: signal transducer activity and MHC class I receptor activity (Table 3). Moreover, another three functions were detected, although with fewer genes, and these were closely

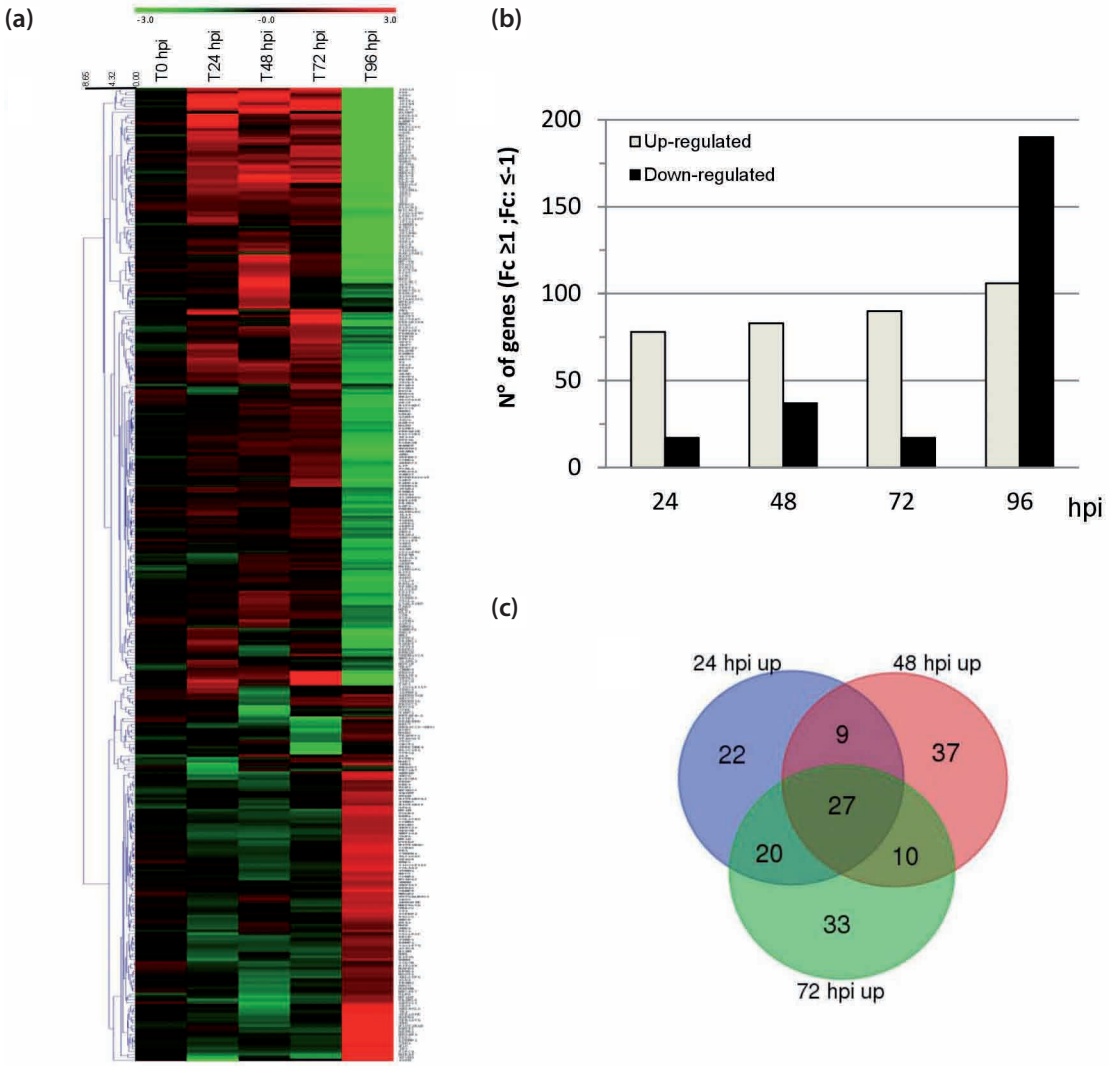

Fig. 1

Transcriptional responses induced by RSV in NCI-H292 cells

RNA from cells was extracted at 0, 24, 48, 72 and 96 hpi. Labeled cDNA was hybridized to HEEBO microarrays (MI, Microarrays Inc.). Microarray data processing is described in Materials and Methods. ANOVA test was performed, resulting in 533 significant probes ($p < 0.01$) corresponding to 339 genes differentially expressed at all time points analyzed. **(a)** Hierarchical clustering (HCL) was performed with TMEV tool v4.7 with 339 genes using Euclidean distance measure. The color is related to the average intensities of every gene at each hpi. The red color represents the up-regulation and green the down-regulation of gene expression as indicated by the scale shown on the top of the heat map. **(b)** Number of genes up- and down-regulated differentially ($p < 0.01$) at 24, 48, 72 and 96 hpi with RSV, filtered according to their intensities (≥1 and ≤-1). This analysis excluded 9 probes named as "orf" or non-coding (total 330 genes). **(c)** Venn diagram comparing the number of up-regulated differentially expressed genes at 24, 48 and 72 h after RSV infection (Fc ≥1 y ≤-1). There are no common genes at 96 hpi.

related to the control of viral infection: double-stranded RNA binding (dsRNA), 2'5' oligoadenylate synthetase (OAS) activity and chemokine activity (Table 3). It is important to note that expression of RIG-I gene, involved in one of the mechanisms of cellular defense to detect dsRNA as well as viral transcripts or genome (Liu *et al.*, 2007) at early stages of infection, also presented significant changes ($p = 0.003$). Nevertheless, it is not included in the list comprising the 27 genes because at 48 hpi its expression was <1 (Fc 0.47), while at 24 and 72 hpi Fcs were 1.38 and 1.54, respectively, and at 96 hpi its expression decreased to -4.31. The OAS genes that belong to the 2'5' oligoadenylate synthetase family associated with viral RNA detection had also a strongly induced expression. Inside this family, although not included in the 27 common genes list, we found the 2'5'oligoadenylate synthetase like (OASL) gene, which presents high levels at 24 and 74 hpi (Fc 2.37 and 2.15, respectively) its expression decreasing at 96 hpi (Fc -5.10).

Table 2. Expression changes of 27 common up-regulated genes (Fc ≥ 1; p value <0.01) between 24, 48 and 72 hpi obtained according to Venn Diagram and expression changes of ISGF3 genes post infection with RSV (changes at 96 hpi are also shown)

Gene symbol	Gene name	Fc			
		24 hpi	48 hpi	72 hpi	96 hpi
IFIT1	interferon-induced protein with tetratricopeptide repeats 1	6.13	2.54	2.73	-6.42
IFI44	interferon-induced protein 44	4.74	1.61	3.41	-5.55
MX1	myxovirus (influenza virus) resistance 1	4.55	3.36	1.70	-6.31
CXCL11	chemokine (C-X-C motif) ligand 11	3.68	1.08	2.39	-3.82
OAS1	2'-5'-oligoadenylate synthetase 1. 40/46kDa	3.41	2.43	2.79	-5.90
OAS2	2'-5'-oligoadenylate synthetase 2. 69/71kDa	2.56	3.07	1.09	-6.96
ISG15	ISG15 ubiquitin-like modifier	2.35	1.45	3.42	-6.86
IFIH1	interferon induced with helicase C domain 1 (MDA5)	2.20	1.67	2.33	-4.14
HLA-A	major histocompatibility complex. class I. A	2.14	3.80	3.42	-4.62
OAS3	2'-5'-oligoadenylate synthetase 3. 100kDa	2.11	1.93	1.27	-4.54
HLA-B	major histocompatibility complex. class I. B	1.93	3.66	3.54	-4.57
IFITM1	interferon induced transmembrane protein 1	1.86	1.78	1.32	-2.86
F3	Thromboplastin	1.78	1.44	1.66	-1.79
HBEGF	heparin-binding EGF-like growth factor	1.68	1.95	1.81	-3.87
HLA-C	major histocompatibility complex. class I. C	1.68	3.06	2.16	-3.80
HLA-F	major histocompatibility complex. class I. F	1.67	2.25	1.97	-3.48
HLA-E	major histocompatibility complex. class I. E	1.63	2.93	2.62	-3.28
WARS	tryptophanyl-tRNA synthetase	1.57	1.14	1.75	-3.93
HLA-H	major histocompatibility complex. class I. H (pseudogene)	1.56	2.67	1.19	-3.66
DDX60L	DEAD (Asp-Glu-Ala-Asp) box polypeptide 60-like	1.55	1.64	1.34	-3.61
B2M	beta-2-microglobulin	1.48	1.59	1.20	-2.15
ZNFX1	zinc finger. NFX1-type containing 1	1.44	1.45	3.55	-3.07
FST	Follistatin	1.36	2.66	2.02	-6.89
STC2	stanniocalcin 2	1.33	1.36	1.01	-2.75
HLA-G	major histocompatibility complex. class I. G	1.13	1.54	2.29	-3.29
IL8	interleukin 8	1.13	1.40	1.31	-3.00
PMAIP1	phorbol-12-myristate-13-acetate-induced protein 1	1.11	1.40	3.17	-3.17
ISGF3 (genes)					
STAT1	signal transducer and activator of transcription 1	2.19	1.68	0.71	-3.58
STAT2	signal transducer and activator of transcription 2	1.39	1.68	0.84	-1.89
IRF9	interferon regulatory factor 9	1.42	0.48	1.35	-2.96

The data is shown using the values of 24 hpi from highest to lowest. hpi: hours post-infection with RSV.

Table 3. GO categories of 27 common up-regulated genes (Fc ≥ 1) between 24, 48 and 72 hpi and genes in these categories (GO enrichment analysis)

	Gene count	Genes	P value
Biological process name			
Cellular response to cytokine stimulus	15	B2M, HLA-A, HLA-B, HLA-C, HLA-E, HLA-F, HLA-G, IFIT1, IFITM1, IL8, ISG15, MX1, OAS1, OAS2, OAS3	$1.0\ e^{-17}$
Cellular response to type i interferon	13	HLA-A, HLA-B, HLA-C, HLA-E, HLA-F, HLA-G, IFIT1, IFITM1, ISG15, MX1, OAS1, OAS2, OAS3	$1.6\ e^{-24}$
Cellular response to interferon-gamma	10	B2M, HLA-A, HLA-B, HLA-C, HLA-E, HLA-F, HLA-G, OAS1, OAS2, OAS3	$1.4\ e^{-16}$
Antigen processing and presentation of exogenous peptide antigen via MHC-I, TAP-independent	7	B2M, HLA-A, HLA-B, HLA-C, HLA-E, HLA-F, HLA-G	$6.0\ e^{-19}$
Molecular function name			
Signal transducer activity	9	FST, HLA-A, HLA-B, HLA-C, HLA-E, HLA-F, HLA-G, HLA-H, IFITM1	$1.0\ e^{-03}$
MHC class I receptor activity	7	HLA-A, HLA-B, HLA-C, HLA-E, HLA-F, HLA-G, HLA-H	$8.5\ e^{-16}$
Double-stranded RNA binding	4	IFIH1, OAS1, OAS2, OAS3	$8.5\ e^{-07}$
2'5' oligoadenylate synthetase activity	3	OAS1, OAS2, OAS3	$1.8\ e^{-08}$
Chemokine activity	2	CXCL11, IL8	$2.9\ e^{-03}$

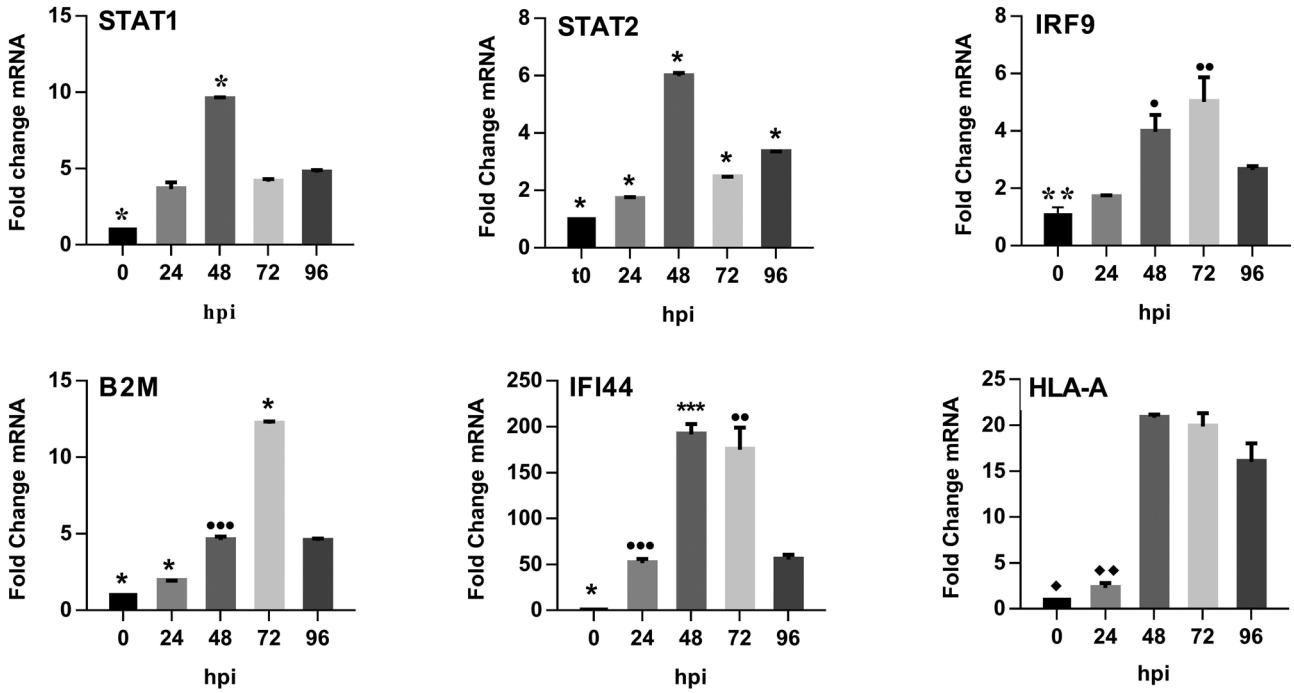

Fig. 2

Relative gene expression of STAT1, STAT2, IRF9, B2M, IFI44 and HLA-A after RSV infection

Relative gene expression was determined by real time RT-PCR using $2^{-\Delta\Delta CT}$ method, HPTR1 was used as housekeeping gene for normalization. Each point was calculated as the mean and standard error of the mean (SEM) of four or five technical replicates. Statistical analysis (ANOVA test) was realized with Sigma Stat 3.5®. *: 0 ≠ 24 ≠48 ≠ 72 ≠ 96 hpi; **: 0 ≠ 48-72 hpi; ***: 48 ≠ 24-96 hpi; •: 48 ≠ 24 hpi; ••: 72 ≠ 24-96 hpi; •••: 24 ≠ 48-72 hpi; ♦: 0 ≠ 48-72-96 hpi; ♦♦: 24 ≠ 48-72-96 hpi.

Relative quantification of ISGF3 complex and selected genes by real time RT-PCR

Taking into account that the most enriched pathways were associated to IFN α/β response, we verified in our infection model whether one of the factors activated by IFN, the transcription factor IFN-stimulated gene factor 3 (ISGF3), was up-regulated. This complex is composed of STAT1, STAT2 and IRF9 (McNab *et al.*, 2015). The microarray analysis showed that these three genes were up-regulated at 24, 48 and 72 hpi and down-regulated at 96 hpi as shown in Table 2. This difference was significant ($p < 0.001$), however because their Fc values were lower than 1 at some experimental time points, they are not included in the list of common genes. We performed real time RT-PCR analysis to obtain a relative quantification of expression of these genes; we detected significant changes after infection as observed in Fig. 2. All these genes presented a peak of expression between 48 and 72 hpi. We also analyzed the expression of 3 common genes: B2M, IFI44 and HLA-A (Table 2), detecting significant changes in their expression ($p < 0.05$). IFI44 and HLA-A had an increased expression between 48 and 72 hpi (Fig. 2). Just as it was for ISGF3 genes, we did not detect a significant decrease in expression of these genes as we observed in microarrays at 96 hpi.

Unique up-regulated genes and GO enrichment analysis

As shown in the Venn Diagram, we detected unique up-regulated genes at 24, 48 and 72 hpi (Fig. 1c). In Table 4 are shown the main GO biological processes, in which these genes are involved and the number of genes detected in each process. The top 10 up-regulated genes are listed in Table 5, depicting the fold changes at each post infection time, including 96 hpi.

At 24 hpi, we found 78 genes having an expression ≥ 1 and 22 of them (28.2%) were only overexpressed at 24 hpi (Fig.1b and c). MMP1 gene had the highest expression in this group (Table 5) and its protein product corresponds to a metalloproteinase that participates in processes of extracellular matrix remodeling (Parks *et al.*, 2004; Ala-aho and Kähäri, 2005). These 22 genes are mainly associated with immune system processes based on the GO enrichment analysis (Table 4). Thus, the greatest proportion of genes (n = 13) was detected in the GO category "defense response" where we found IFI35, IFIT5, IL1A, IL1RL1, ITGB1, MST1R, NMI, PARP9, PLSCR1, PSMB8, TRIM22, UBA7 and USP18. Among them, IFI35, PARP9, TRIM22 and IL1RL1 presented the highest activation as shown in Table 5.

At 48 hpi, we detected 83 genes with an expression ≥ 1 and 37 of them were up-regulated only at 48 hpi (Fig. 1b and c).

The ALX3 gene, a transcriptional regulator (Perez-Villamil*et al.*, 2004), presented the highest activation (Table 5). Considering the GO enrichment pathways, in which these 37 genes are included, apart from the immune response pathways, it is worthy to note that genes that participate in apoptotic processes were up-regulated (Table 4). Genes belonging to the immune system process were ADAR, AQP3, BPIFA1, CXCL1, DUSP4, EIF2AK2, IFI44L, LCN2, OSTM1, RICTOR, S100A8, S100A9, TCF7 and VEGFA. The genes that presented the top activation in this process were BPIFA1 (Fc 2.70) and S100A9 (Fc 2.27). On the other hand, genes detected under the label "regulation of apoptotic process" were ADAR, ALX3, HTRA2, IGFBP3, LCN2, PTGS2, S100A8, S100A9, TCF7 and VEGFA, where ALX3, S100A9, LCN2 and TCF7 showed the greatest fold changes of 4.08, 2.27, 2.17 and 2.10, respectively.

At 72 hpi, we detected 90 genes presenting the expression ≥1, among them 33 (36.7%) are up-regulated only at this time. The highest expression was found in SLC30A7 and PPP1R15A, as shown in Table 5. The gene SLC30A7 is associated with a cation transmembrane transporter activity and transport to the Golgi (Kirschke and Huang, 2003), while PPP1R15A or GADD34 codes for a protein that responds to genomic damage activating apoptosis (Yagi *et al.*, 2003). The main pathways encompassing the 33 genes are listed in Table 4. Among them stand out both response to endogenous stimulus and response to hormone stimulus. In this last process were found the genes CDKN1A, PCSK9, FOSL1, CCND1, TXNIP, TRIB3, ABCC8, LDLR, AHR. Both CDKN1A and PCSK9 presented the top activations with Fc values of 2.02 and 1.85, respectively. CDKN1A (known as P21/WAF) codes for a potent cyclin-dependent kinase inhibitor promoting cell cycle arrest in response to a variety of stimuli (Karimian*et al.*, 2016) and PCSK9 belongs to the convertase family, family of proteases that process protein and peptide precursors trafficking through the secretory pathway (Seidah and Prat, 2012).

At 96 hpi, we found 122 up-regulated genes out of 330 (37.5%), among them 106 presented changes ≥1. As mentioned before, we did not detect any genes co-upregulated with all other pi times. We detected one common gene with 48 hpi (GLA) and four genes with 72 hpi (ANKRD36, ABCC8, PRSS23 and MAP2). No common genes were present when compared to 24 hpi. Top ten genes having the highest expression are listed in Table 5, and all of them presented changes >3. The ATOH8 gene is on the top of the list at 96 hpi and codes for a transcription factor involved in differentiation processes (Chen *et al*, 2011). The main biological processes, in which these 106 genes participate, are shown in Table 4. Unlike the up- regulated pathways at previous pi times, at 96 hpi there is activation of cell processes related to cell cycle and cytoskeleton rearrangement. This probably accounts for cell processes associated with cellular restructuring caused by the viral infection, such as the syncytia formation. The genes that presented the highest changes under the process "mitotic cell cycle" were TOP2A, UBD, NUSAP1, TPX2, CDK1 and ASPM (Supplementary Table S1). On the other hand, in the process "microtubule cytoskeleton organization" we detected, apart from NUSAP1, TPX2 and CDK1, the genes STMN1, CKS2, UBE2C, SPAG5, ZWINT, CCNB1, TACC2 and with lower change PRC1 and MAP2 (Supplementary Table S1).

Table 4. GO categories of up-regulated (Fc ≥ 1) and down-regulated (Fc ≤ -1) unique genes obtained at 24, 48, 72 and 96 hpi after Venn Diagram analysis

GO: Biological process name	Gene count	P value
Up-regulated		
24 hpi (n: 22 genes)		
Defense response	13	$5.8e^{-08}$
Response to cytokine stimulus	9	$1.4e^{-06}$
Innate immune response	9	$1.9e^{-06}$
Cytokine-mediated signaling pathway	7	$2.0e^{-05}$
48 hpi (n: 37 genes)		
Inmune system process	14	$1.6e^{-03}$
Defense response	12	$1.0e^{-03}$
Regulation of apoptotic process	10	$5.0e^{-03}$
Leucocyte migration involved in inflammatory response	2	$5.0e^{-03}$
72 hpi (n: 33 genes)		
Response to hormone stimulus	9	$2.1e^{-03}$
Response to lipid	8	$2.1e^{-03}$
Response to organic nitrogen	8	$2.1e^{-03}$
96 hpi (n: 106 genes)		
Cell cycle phase	21	$1.6e^{-05}$
Mitotic cell cycle	19	$3.1e^{-05}$
Mitosis	13	$4.8e^{-05}$
Microtubule cytoskeleton organization	12	$2.7e^{-05}$
Down-regulated		
24 hpi (n: 17 genes)		
Nervous system development	9	$2.3e^{-05}$
48 hpi (n: 37 genes)		
Response to organic nitrogen	5	$1.4e^{-02}$
Response to molecule of bacterial origin	3	$1.7e^{-02}$
Regulation of interleukin-8 production	2	$3.2e^{-03}$
72 hpi (n: 17 genes)		
RNA processing	3	$1.8e^{-02}$
Golgi vesicle transport	2	$1.1e^{-02}$
96 hpi (n: 189 genes)		
Innate immune response	55	$3.1e^{-36}$
Response to virus	43	$4.6e^{-37}$
Response to type i interferon	26	$4.8e^{-32}$

n: number of genes submitted to GO enrichment analysis ($p < 0.05$).

Genes down-regulated at every single post infection time

In the group of down-regulated genes, we did not detect any common genes that keep a diminished expression pattern

Table 5. Expression changes of unique genes (top ten, up and down-regulated) obtained per time after RSV infection according to Venn Diagram analysis (Fc: ≥ 1, ≤ -1)

24hpi		48 hpi		72 hpi		96 hpi	
Gene symbol	**Fc**	**Gene symbol**	**Fc**	**Gene symbol**	**Fc**	**Gene symbol**	**Fc**
Up-regulated genes							
MMP1	3.38	ALX3	4.08	SLC30A7	3.08	ATOH8	4.18
REC8	2.08	CCL4L2	3.66	PPP1R15A	3.02	TOP2A	3.93
IFI35	1.93	MTX1	3.12	ATF3	2.24	GPR109A	3.62
PARP9	1.73	CPSF1	2.77	CDKN1A	2.02	PHTF2	3.58
TRIM22	1.60	PLUNC	2.70	TFPI2	2.00	UBD	3.53
CDH23	1.56	ISPD	2.33	SOX9	2.00	HIST1H1B	3.51
IGFBP1	1.54	RAB3IL1	2.32	PCSK9	1.85	MXRA5	3.44
IL1RL1	1.49	EGFL8	2.31	PARP14	1.84	NUSAP1	3.39
SAMD9L	1.47	S100A9	2.27	TXNIP	1.76	ID3	3.21
MST1R	1.42	LCN2	2.17	CARS	1.74	TPX2	3.20
Down-regulated genes							
ASPM	-4.26	OCRL	-2.50	CCT6A	-3.11	PLUNC	-5.69
INHA	-2.11	MYO9A	-2.37	BLOC1S1	-2.46	STC1	-5.39
DNAJC2	-1.86	UIMC1	-2.16	CNOT1	-2.46	RAP1GAP2	-5.28
TBC1D7	-1.72	ZNF823	-1.87	SERPINB4	-2.36	OASL	-5.11
TCTN1	-1.65	MT1DP	-1.86	RCN2	-2.04	MX2	-4.57
NNMT	-1.46	CD59	-1.77	RPL7	-1.71	GDF15	-4.37
ETV4	-1.29	IGFBP1	-1.65	DNAJC25	-1.50	RIG-**I**	-4.31
NOTCH3	-1.29	KRTAP4-6	-1.59	MSH6	-1.50	IFI44L	-4.17
MAP2	-1.20	ANXA8L1	-1.55	STAG3L3	-1.25	PRIC285	-4.12
SNCG	-1.16	TLR9	-1.54	CTSC	-1.23	DUSP4	-4.01

among the 4 post infection times, and only the MXRA5 gene was inhibited at 24, 48 and 76 hpi (Fc -1.32, -1.00, -1.58, respectively). Nevertheless, at 96 hpi this same gene was up-regulated (Fc 3.44). MXRA5 codes for a protein related to extracellular matrix remodeling (Walker and Volkmuth, 2002).

At 24 hpi, we detected 131 genes out of 330 that were inhibited (40 %), with only 17 genes that presented Fc <-1. TRIM29 and AHNAK genes were down-regulated at both 24 (Fc -1.29 and -1.64, respectively) and 48 hpi (Fc -1.57 and -1.41, respectively). ATOH8 gene was common between 24 and 72 hpi (Fc -2.03 and -1.75, respectively), being one of the genes showing the highest inhibition at 24 hpi. Top ten genes down-regulated only at 24 hpi are shown in Table 5. Due to the low number of genes with Fc< -1, the main pathway detected in the GO enrichment analysis was associated with genes belonging to the nervous system development family (Table 4), comprised of nine genes: AHNAK, ANK3, ASPM, ATOH8, ETV4, INHA, MAP2, NOTCH3 and TCTN1. Among them, ASPM, a gene associated with mitotic spindle regulation, presented the highest inhibition (Table 5) (Higgins *et al.*, 2010).

At 48 hpi, 131 genes (39.7%) were down-regulated, 37 of them presented an expression ≤ -1. The genes having the greatest changes are shown in Table 5. OCRL gene presented the highest inhibition, and has been described in several processes such as regulating membrane trafficking and primary cilium formation (Madhivanan *et al.*, 2015). When these 37 genes were analyzed, there were only a few biological processes enriched. As shown in Table 4, the main biological process is linked to the response to organic nitrogen with the genes included: ABCC8, IGFBP1, MGST1, PTPRF, and TLR9.

At 72 hpi, we detected 118 down-regulated genes that corresponded to 35.8% of total genes with significant changes in expression after infection. Only 17 of them exhibited changes lower than -1. PSIP1 presented the highest decrease in expression (Fc -3.38). This gene associates with the function "RNA polymerase II" and is also inhibited at 48 hpi (Fc -1.04) (Singh *et al.*, 2001). As shown in Table 5, we detected that CCT6A is the gene that presented the highest decrease of expression; the protein coded by this gene has a chaperone role and assists the folding of proteins, especially actin and tubulin (Mukherjee *et al.*, 2010). In the GO enrichment analysis, only two biological processes were enriched: RNA processing and Golgi vesicle transport, although with a few genes belonging to each one: CNOT1, PSIP1 and RPL7 to the first pathway (Fc in Table 5) and TRAPPC1 (Fc -1.21) and BLOC1S1 (Fc -2.46) to the second.

At 96 hpi, we found a higher percentage of down-regulated genes compared to all other times after infection analyzed. The genes up-regulated between 24–72 hpi were turned off at 96 hpi. Thus 208 out of 330 differentially expressed genes showed a reduced expression and 189 of them had Fc ≤ -1. The genes with highest changes are shown in Table 5, but we excluded OAS2, FST, IGS15, IFIT1, MX1, OAS1 and IFI44, because these genes were included in the Table 2 (common genes). In addition, 189 genes were associated with a biological process related to immune response by the GO enrichment analysis (Table 4), showing a control of the antiviral mechanism attenuating several other pathways. In GO category "response to virus", we detected 43 of 189 genes (22.8%). Among them 8 genes belonged uniquely to this pathway and were not included in the other two categories (Venn Diagram analysis). These genes were IFI44, IFI44L, IL6, EIF2AK2, TRIM22, FOSL1, GBP3, and TRIM5 (Fc are in Supplementary Table S1).

Discussion

The respiratory syncytial virus is the main etiologic agent of lower respiratory tract infections in infants. In Chile, in a study on healthy term infants younger than 6 months with acute LRTI, 59.7% of patients presented an infection due to RSV and 22.6% a co-infection (Luchsinger *et al.*, 2014). Most symptomatic cases consult 2 to 3 days after the symptoms have started and for this reason, *in vitro* models that cover greater infection timing can contribute to a better understanding of virus pathogenesis.

Our aim was to analyze temporal changes in cellular gene expression after infection by RSV using the human cell line derived from lung, NCI-H292, that is a continuous human lung muco-epidermoid cell line permissive to infection by RSV and other human paramyxoviruses. We analyzed expression changes at 4 times after infection, namely 24, 48, 72 and 96 h at a low multipilicity of infection, 5 Log PFU/ml, approximately 0.1 MOI. This log PFU/ml value is similar to those reported in the literature in nasal samples of RSV infants. In the study performed by ElSaleeby *et al*. the mean nasal viral load was of 4.63 log PFU/ml in children under 1 year old on the first day of enrollment (ElSaleeby *et al.*, 2011). Similar RSV load values have been previously obtained by DeVicenzo. In this study, RSV-A load was of 4.77 log PFU/ml in nasal wash in a hospitalized infant upon enrollment. The y-intercept of the regression line for RSV-A was of 5.27, suggesting that this viral load would be at the onset of symptoms (Day 0) (DeVincenzo, 2004). In a follow-up study of hospitalized RSV-infants younger than 1 year old, they also detected similar viral loads, approximately 6 log PFU/ml at the time of admission (Brint *et al.*, 2017). This background indicates that the inoculum used in our study measured as log PFU/ml is comparable to *in vivo* situations, when we consider hospitalized infants, a risk group, whose dynamics of infection is important to understand. Although the MOI used represents a low density of infection when expressed in terms of number of cells, we have no possibility of extrapolating it to *in vivo* values. Despite this low MOI, we confirmed the presence of RSV by IFA and real time RT-PCR; nevertheless we were not able to observe syncytia formation, just cell clusters. Previus data have shown that NCI-H292 cell line presents a delayed cytopathic effect when compared to the cell lines HeLa-I and HEp-2 after RSV infection. NCI-H292 cell line showed a lower number of isolations (52%) but it presented a better cell stability (Perini*et al.*, 2007). This cell line has also been used as a model for inflammation induction by several agents that affect lungs, with similar response as the primary lung epithelial cells (Newland and Richter, 2008). Thus, NCI-H292 cell line could be a viable model for studying the effects of RSV infection on gene expression at longer infection times.

Previous studies of gene expression after RSV infection in different cell models using microarrays have been reported. A lower airway epithelial cell A549, type II alveolar cells and a single post infection time have been used in several studies (Zhang *et al.*, 2001, 2003; Tian *et al.*, 2002). Only in the study of Martinez *et al*, they carried out a follow up of 3 hpi at 6, 12 and 24 h with an inoculum of RSV of 3 PFU, close to that used in our study (Martínez *et al.*, 2007). Other studies have used human bronchial epithelial cell BEAS-2B; in the work by Huang *et al.* they performed the analysis at 4 and 24 hpi, while Mayer *et al.* only at 4 hpi, both used MOI of 1 (Mayer *et al.*, 2007; Huang *et al.*, 2008).On the other hand, Janssen used an animal model. They inoculated BALBc/mice and analyzed the expression profile in lung tissue at 1 and 3 days post infection (Jannsen *et al.*, 2007).

Therefore, most of the published studies do not perform a follow up of the cellular response after RSV infection and with our study is only comparable what happens at 24 hpi. In addition, variations on the type of microarrays used and MOI may result in differences between our results and those obtained by other groups of researchers.

In our study, we identified 330 differentially expressed genes at 4 post infection times with RSV by microarray. We obtained different expression patterns, a bi-phasic gene expression profile, with a predominantly down-regulated profile at 96 hpi compared to earlier hpi. This pattern is maintained when considering the genes with changes ≥1 or ≤-1. About 60% of the genes were up-regulated between 24–72 hpi. This early gene expression pattern showed a rapid and sustained activation of several genes after RSV infection and then turned off at 96 hpi. This change is possibly due to the viral replication and cellular anti-viral response. A previous report by Martinez indicates an early activation at 6 hours post infection (Martínez *et al.*, 2007). It is known that specific

viral proteins such as NS1 and NS2 can interact with cellular pathways to block the anti-viral effect of the cell (Barik, 2013; Schmidt and Varga, 2017). Although in our study we did not evaluate the presence of these viral proteins, unpublished results from our group with an infection at MOI of 1 in this cell line have revealed that the maximum viral replication is reached at 96 hpi. This could indicate a possible involvement of RSV replication in counteracting the anti-viral response of the cell by decreasing the expression of innate immune response genes as we observed at 96 hpi.

Between 24–72 hpi, we detected an up-regulated gene expression pattern. Twenty-seven genes remained up-regulated (Fc ≥ 1) at 24, 48 and 72 hpi. These genes are mainly related to innate immune response, highlighting the activation of dsRNA sensors, IFN producing pathways, IFN- stimulated pathways, and pathways associated to antigen presentation. Viral infection is first detected by sensors such as RLRs, which include RIG-I and IFIH1 (MDA5) (Goubau *et al.*, 2013). In our study, the levels of IFIH1 detected were higher than RIG-I although the temporality was similar, both presenting a decrease at 96 hpi. Other reports have suggested that the main activated pathway after RSV infection is RIG-I. Liu and colleagues found binding of viral RNA only to RIG-I and not to IFIH1 (Liu *et al.*, 2007). These apparent divergences can be explained given the different cell lines and MOI that were used. However, in murine lung tissue a great activation of IFIH1 is detected at 24 hpi and remains up-regulated at 3 days post infection (Janssen *et al.*, 2007). RSV has generated mechanisms to counteract RIG-I and IFIH1 action. The RSV NS2 protein is able to interact with RIG-I, blocking its action (Ling *et al.*, 2009), while in infected HEp2 cells at 12 hpi, IFIH1, MAVS and the viral protein N were co-localized in inclusion bodies, the primary site for viral RNA replication (Lifland *et al.*, 2012). Sequestering of IFIH1 could diminish IFN expression. Facing these virus adaptation mechanisms, the cell probably induces a sustained activation of IFIH1 and RIG-I expression during the 72 hpi, as we observed in our cell model.

The pathways of viral infection recognition through IRF3 and IRF7 activate the expression of type I IFNs (IFN α and β) and ISGs that trigger inflammation signals and chemoattraction of immune response cells in order to control the infection (Takaoka and Yanai, 2006). Although we did not detect changes in the expression of IRF3 and IRF7, neither we detected IFNα and IFNβ mRNAs, we did detect genes of pathways that respond to these signals. One of them, widely described by its antiviral action, is the transcription complex IGSF3 that translocates to the nucleus and binds to different promoters that respond to interferon (ISRE) (Fink and Grandvaux, 2013; McNab *et al.*, 2015). We detected a significant increase of STAT1, STAT2 and IRF9 mRNA levels that comprise this complex, from 24 until 72 hpi. Although via real time RT-PCR we did not find an abrupt decrease in expression at 96 hpi as the one detected by microarrays, we indeed observed a decrease in mRNA levels at 96 hpi. This could be due to technical differences regarding the amount of mRNA used in each technique and the amplification region selected in real time RT-PCR, as in microarray assay several probes target each mRNA. STAT1 expression was the highest compared to the other two genes. In studies using STAT1 KO mice, there has been observed an increased susceptibility to infections with different bacteria and viruses, including ssRNA negative virus like vesicular stomatitis virus (VSV), however, there are no reports about RSV infection (Boisson-Dupuis *et al.*, 2012). It is well established that ISGF3 responds to IFN α and β stimuli so we suggested in our cell model of RSV infection that the virus is able to activate the IFN pathway as observed in other studies. In the study by Jannsen and colleagues using a murine model, they also detected up-regulation of STAT1 and STAT2 genes at days 1 and 3 after infection, STAT1 being the one with the highest activation (Janssen *et al.*, 2007). In infants with LTRI caused by influenza or RSV infection, STAT1 and STAT2 activation is detected systemically (Mejías *et al.*, 2013). RSV proteins NS1 and NS2 can affect the formation of ISGF3 by sequestering STAT2 and resulting in its degradation (Lo *et al.*, 2005; Swedan *et al.*, 2009, 2011). RSV is able to suppress the both the IFN production pathway and the IFN effector pathway. This could explain the pattern of different expression between 24–72 hpi and 96 hpi.

It is known that there are many genes whose expression is dependent on IFN, triggered downstream of the IFN receptor. Among the 27 up-regulated common genes, several belong to these signaling pathways. IFIT1 (ISG56) is one of the genes with highest response to IFN. The Fc was the highest among the common genes at 24 hpi. It has also been detected in the murine model, showing one of the major changes on day 1 post infection (Janssen *et al.*, 2007). IFIT1 acts by sensing viral RNA (Fensterl and Sen, 2015). Among the mechanisms of anti-viral action of IFIT1 has been described an inhibitory action on the initiation of translation by its interaction with eIF3 (Fensterl and Sen, 2011). It is also able to recognize 5-mRNA ends, whose caps lack 2'-O-methylation of the first ribose, competing with eIF4E to block the translation of viral mRNAs bearing those features. IFIT1 also binds and sequesters 5' triphosphorylated RNAs that are at the 5' ends of genomic and non-genomic RNA of some RNA viruses altering the viral replication. A study by Barik determined that 5' terminal cap structure of RSV mRNA is the cap 0 type and has no 2'-O methylation on the first ribose (Barik, 1993). This structure might be the target for IFIT1 and its expression activation would be an important antiviral mechanism. In studies using coronavirus lacking the 2' O-methyl transferase activity, a higher susceptibility to the IFIT1 action controlling the infection has been observed (Diamond, 2014; Menachery *et al.*, 2014). It is unknown

whether RSV has some counteracting mechanism for the lack of 2'-O-methylation in its mRNAs, although RSV protects its genomic RNA through the binding of viral protein N, which it covers completely, creating an RNase-resistant nucleocapsid (Collins *et al*., 2013).

Identification of foreign RNAs is an antiviral response also performed by enzymes that are activated by dsRNA and belong to the family of ISGs (Kristiansen *et al*., 2011). In our experiments we detected an increase in expression of oligoadenylate synthetases(OAS1, OAS2 and OAS3). This increase was higher at 24 hpi for OAS1, although it remained increased until 72 hpi. Similar, in the infant study there is an increased expression of OAS1 and to a lesser extent of OAS2.This last study was performed between 24 to 72 hours after admission into the hospital (Mejías *et al*., 2013). In addition, both in the murine model and A549 cells infected with RSV, an increase in mOas1a and OAS2 has also been detected at 24 hpi (Janssen *et al*., 2007; Martínez *et al*., 2007).These enzymes synthesize 2'-5' oligoadenylates activating a latent RNase, RNase L, to induce RNA degradation, resulting in the inhibition of viral replication. On the other hand, in this family we find OASL. This protein, unlike OASs, has no enzymatic activity so its mechanism of antiviral action remains elusive. OASL contains two tandem ubiquitin-like domains (UBL) at the C-terminus and this domain is absent in OASs. We detected increased OASL expression at 24 and 72 hpi and it decreased at 96 hpi. It has been proposed that OASL could bind to the pUb site of RIG-I, thereby increasing the sensitivity to detect RNAs (Zhu *et al.,* 2015). The involvement of OASL and particularly the importance of UBL domain in the response against RSV has been demonstrated using HEK293 cells with constant expression of OASL (Dhar *et al*., 2015). In the whole blood microarrays study on infants, the activation of OASL was detected following RSV infection in a higher proportion than the other genes of the family (Mejias *et al*., 2013).These results suggest an important participation of this pathway in the early control of infection.

In the common genes group we also detected an important up-regulation of IFI44, a gene induced by IFN α and β. In murine lung tissue infected with RSV, a strong activation was obtained at 24 hpi, diminishing at day three (Janssen *et al*., 2007). Both Fjaerli and Mejías detected an increased expression of IFI44 at a systemic level in infants hospitalized due to RSV infection (Fjaerli*et al*., 2006; Mejías *et al*., 2013). The role of this strong up-regulation and its involvement in the control of the infection is not known; only in the model of HIV infection it has been demonstrated that IFI44 inhibited viral replication (Power *et al.,* 2015).

Other group of strongly up-regulated genes corresponds to HLA, associated to antigen recognition. $CD8^+$ cytotoxic T lymphocytes recognize the antigens presented by class I HLA molecules, the activation of these immune cells allows the control of infection but they also participate in the generation of lung damage after RSV infection. Class i HLA molecules correspond to a heterodimer that includes B2M that appeared differentially expressed in our study. In the report of Guo *et al.* (2015) in A549 cells with MOI similar to ours they did not detect significant changes of HLA-A, HLA-B or HLA-C at 36 hpi. However, when using a MOI of 0.3 or 1.0 they detected changes in gene expression and cell surface protein expression. In this model, they propose a modulation of HLAs expression through the activation of NLRC5 via RIG-I/IFNβ (Guo *et al.,* 2015). Previous studies have already demonstrated the important role of IFNβ in modulating that expression (Garofalo *et al*, 1996). An increase of HLA-B and E has also been observed in A459 cells at 24 hpi (Martínez *et al*., 2007). In our model, we detected higher activation of HLA-A/B/C/E/F/H expression at 48 hpi of RIG-I. Considering the involvement of these molecules in antigen presentation, such activation was expected; however, we are not able to explain what is the biological consequence of activation of several HLA. On the other hand, B2M expression has been used as a reference gene (Radonić *et al.*, 2004), but our data show significant changes in its expression at all hpi analyzed. Accordingly, when performing relative expression studies in viral infection models, it is necessary to consider that the antigen presentation pathway, where B2M is involved, is strongly regulated and this gene does not have a stable expression to be used as a reference gene.

One of the consequences of infection is the inflammatory response activation. In our study, we detected one of the highest up-regulations the up-regulation of CXCL11, and to a lesser extent IL8. Both in A549 cells and murine lung tissue detect activation as well of CXCL11 expression mainly at 24 hpi (Janssen *et al*., 2007; Martínez *et al.*, 2007). It is known that epithelial cells release recruitment mediators of immune cells to the infection site; although CXCL11 belongs to the chemokines family, the direct effect of CXCL11 on RSV infection is unknown (Farrag and Almajhdi, 2016). On the other hand, in our model, IL8 expression, one of the most important mediators of the inflammatory response, had a slight increase over time; however, it has been observed that there is a significant production of this neutrophil chemoattractant at a systemic level and in the respiratory tract (Farrag and Almajhji, 2016; Rusell *et al*., 2017). In infants younger than 6 months infected with RSV, an increased amount of IL8 has been detected at a systemic level. In addition, this chemokine is present in higher concentrations in RSV-infants with severe LTRI compared with controls or RSV-infants with moderate disease (Larrañaga *et al*., 2009). The difference between the expression obtained in our cell line and the systemic levels might be due to the fact that many other cells, especially the immune system cells, are able to release this chemokine during infection and its expression is not restricted to the epithelial cells.

When analyzing the pathways, in which the individual genes were activated at each time after infection, we observed mainly an activation of the immune response pathway at 24 and 48 hpi. However, at 48 hpi is also present the activation of genes that modulate apoptosis. At 72 hpi, we detected genes associated with response to several stimuli such as hormones, lipids and organic nitrogen. At 96 hpi, we also detected a second expression pattern; over 120 genes, which remained silenced until 72 hpi, were steeply up-regulated by 96 hpi. A great proportion of these genes was related to cell cycle, mitosis and microtubules rearrangement. Up-regulation of these genes was expected considering the morphological changes that cells experience after infection and the clustering we observed, all changes that should require signals for cytoskeleton rearrangement. It is known that the virus must need the cell cytoskeleton to allow assembly of viral proteins and genome and liberation from host cells (budding), therefore, knowing that in our cell model, there is a greater viral replication associated with greater viral particles release between 72 and 96 hpi, it is highly possible that the virus modulates the signals in order to be released (Shahriari *et al*., 2016).

Although we detected up-regulated genes at 96 hpi, the expression pattern at that time was mainly down-regulated. These genes were associated with the innate immune response, including genes associated with virus response and IFN type I response. Among these genes are included several of the common genes activated at 24, 48 and 72 hpi as shown in Table 2. OAS2 and ISG15 were the genes that presented the strongest down-regulation. As we previously mentioned, OAS2 is associated with the recognition pathway of viral RNAs to induce their degradation. The virus responds against the cell antiviral response using several mechanisms. One of them is related to sequestering of cellular proteins by viral proteins, interfering with different pathways of the innate immune response (Wu *et al*., 2012; Schmidt and Varga, 2017). It has been observed that RSV NS1 sequesters IRF3, interfering with its transcriptional activity associated with IFN and possibly reflects a decrease in the expression of genes associated with that pathway (Ren *et al*., 2011). Considering that a peak of viral replication is observed in NCI-H292 cells at 96 hpi when using a MOI of 1 (personal communication), the greatest amount of viral proteins such as NS1 at this time may block the ISGs expression. This could support the highest proportion of down-regulated genes detected at 96 hpi.

ISG15 is the second most down-regulated gene at 96 hpi. This gene codes for an ubiquitin-like protein that modifies other proteins. Several proteins are ISGylated in the response to interferon during viral infection, altering their function (Morales and Lenschow, 2013; Zhao *et al*., 2013). ISG15$^{-/-}$ KO mice are more susceptible to infection by Sendai virus and influenza a and B virus. Nevertheless, ISG15's antiviral action would not associate with the inhibition of viral replication but with protein ISGylation (Morales *et al*., 2015).This last mechanism has also been described in the RSV infection of A549 cells and A549 ISG15$^{-/-}$.The antiviral effect of ISG15 would be evident in cells having a high amount of ISG15 before virus infection, namely those cells stimulated by interferon released by the infected cells (González-Sanz *et al*., 2016). In a murine lung epithelial cells model (MLE-15), an increase of ISG15 after RSV infection is observed, this increment is higher when the infection is performed using RSV without the G protein (ΔG), suggesting a control of G protein over ISG15 expression (Moore *et al*., 2008). ISG15 appears to be an important mediator of the antiviral response of RSV as well other viral infections (Zhao *et al*., 2013).

Using NCI-H292 cellular model of infection, we detected many up-regulated genes between 24 to 72 hpi. Among them, 27 genes remain are highly up-regulated, suggesting an important participation in the control of viral infection. It has been mainly described that the proteins coded by these genes participate in the innate immune response pathways associated with the activation of IFN α and β and ISGs. Many of them have been detected increased in circulation of RSV infants. Other pathways are up-regulated more extensively at each post infection time, such as the regulation of apoptotic processes at 48 hpi and mitotic processes and organization of the cytoskeleton at 96 hpi; they could be related to the changes that RSV induces at the cellular level during its replication. Although we did not perform quantification of the viral load, studies carried out by us and others have determined interference of the RSV proteins with the cellular antiviral response; these interactions possibly affect the transcription of cellular genes involved in that response. Our cellular model will allow us to carry out future studies by analyzing cellular pathways that have relevance in the elimination of the virus at later times after infection, as well as studying specific pathways that are differentially expressed in RSV-infected infants showing a different infection severity.

Acknowledgments. This work was funded by the Research Project Fondecyt N°11070254 granted to S.A. by the Office of Science and Technology Development of the Chilean Government. We want to thank Dr. Pedro Piedra (Baylor College of Medicine, Houston, TX, US) for kindly providing RSV/A/Tracy via Dr. Luis Avendaño, Virology Program, Institute of Biomedical Sciences, Faculty of Medicine, University of Chile.

Supplementary information is available in the online version of the paper.

References

Ala-aho R, Kähäri VM (2005): Collagenases in cancer. Biochimie 87, 273–286. https://doi.org/10.1016/j.biochi.2004.12.009

Ampuero S, Luchsinger V, Tapia L, Palomino MA, Larrañaga CE (2011): SP-A1, SP-A2 and SP-D gene polymorphisms in severe acute respiratory syncytial infection in Chilean infants. Infect. Genet. Evol. 11, 1368–1377. https://doi.org/10.1016/j.meegid.2011.04.033

Avendaño LF, Palomino MA, Larrañaga C (2003): Surveillance for respiratory syncytial virus in infants hospitalized for acute lower respiratory infection in Chile (1989 to 2000). J. Clin. Microbiol. 41, 4879–4882. https://doi.org/10.1128/JCM.41.10.4879-4882.2003

Barik S (1993): The structure of the 5' terminal cap of the respiratory syncytial virus mRNA. J. Gen. Virol. 74, 485–490. https://doi.org/10.1099/0022-1317-74-3-485

Barik S (2013): Respiratory syncytial virus mechanisms to interfere with type 1 interferons. Curr. Top. Microbiol. Immunol. 372, 173–191.

Boisson-Dupuis S, Kong XF, Okada S, Cypowyj S, Puel A, Abel L, Casanova JL (2012): Inborn errors of human STAT1: allelic heterogeneity governs the diversity of immunological and infectious phenotypes. Curr. Opin. Immunol. 24, 364–378. https://doi.org/10.1016/j.coi.2012.04.011

Brint ME, Hughes JM, Shah A, Miller CR, Harrison LG, Meals EA, Blanch J, Thompson CR, Cormier SA, DeVincenzo JP (2017): Prolonged viral replication and longitudinal viral dynamic differences among respiratory syncytial virus infected infants.Pediatr Res. 82, 872–880. https://doi.org/10.1038/pr.2017.173

Chen M, Hu KF, Rozell B, Orvell C, Morein B, Liljeström P (2002): Vaccination with recombinant alphavirus or immune-stimulating complex antigen against respiratory syncytial virus. J. Immunol. 169, 3208–3216. https://doi.org/10.4049/jimmunol.169.6.3208

Chen J, Dai F, Balakrishnan-Renuka A, Leese F, Schempp W, Schaller F, Hoffmann MM, Morosan-Puopolo G, Yusuf F, Bisschoff IJ, Chankiewitz V, Xue J, Chen J, Ying K, Brand-Saberi B (2011): Diversification and molecular evolution of ATOH8, a gene encoding a bHLH transcription factor. PLoS One 6, e23005. https://doi.org/10.1371/journal.pone.0023005

Collins PL, Fearns R, Graham BS (2013): Respiratory syncytial virus: virology, reverse genetics, and pathogenesis of disease. Curr. Top. Microbiol. Immunol. 372, 3–38. https://doi.org/10.1007/978-3-642-38919-1_1

Collins PL, Melero JA (2011): Progress in understanding and controlling respiratory syncytial virus: still crazy after all these years. Virus Res. 162, 80–99. https://doi.org/10.1016/j.virusres.2011.09.020

DeVincenzo JP (2004): Natural infection of infants with respiratory syncytial virus subgroups A and B: a study of frequency, disease severity, and viral load. Pediatr. Res. 56, 914–917. https://doi.org/10.1203/01.PDR.0000145255.86117.6A

Dhar J, Cuevas RA, Goswami R, Zhu J, Sarkar SN, Barik S (2015): 2'-5'-Oligoadenylate synthetase-like protein inhibits respiratory syncytial virus replication and is targeted by the viral nonstructural protein 1. J. Virol. 89, 10115–10119. https://doi.org/10.1128/JVI.01076-15

Diamond MS (2014): IFIT1: A dual sensor and effector molecule that detects non-2'-O methylated viral RNA and inhibits its translation. Cytokine Growth Factor Rev. 25, 543–550. https://doi.org/10.1016/j.cytogfr.2014.05.002

El Saleeby CM, Bush AJ, Harrison LM, Aitken JA, DeVincenzo JP (2011): Respiratory syncytial virus load, viral dynamics, and disease severity in previously healthy naturally infected children. J. Infect. Dis. 204, 996–1002. https://doi.org/10.1093/infdis/jir494

Farrag MA, Almajhdi FN (2016): Human respiratory syncytial virus: role of innate immunity in clearance and disease progression. Viral Immunol. 29, 11–26. https://doi.org/10.1089/vim.2015.0098

Fensterl V, Sen GC (2011): The ISG56/IFIT1 gene family. J. Interferon Cytokine Res. 31, 71–78. https://doi.org/10.1089/jir.2010.0101

Fensterl V, Sen GC (2015): Interferon-induced IFIT proteins: their role in viral pathogenesis. J. Virol. 89, 2462–2468. https://doi.org/10.1128/JVI.02744-14

Fink K, Grandvaux N (2013): STAT2 and IRF9: Beyond ISGF3. JAKSTAT 2, e27521. https://doi.org/10.4161/jkst.27521

Fjaerli HO, Bukholm G, Krog A, Skjaeret C, Holden M, Nakstad B (2006): Whole blood gene expression in infants with respiratory syncytial virus bronchiolitis. BMC Infect. Dis. 6, 175. https://doi.org/10.1186/1471-2334-6-175

Garofalo R, Mei F, Espejo R, Ye G, Haeberle H, Baron S, Ogra PL, Reyes VE (1996): Respiratory syncytial virus infection of human respiratory epithelial cells up-regulates class I MHC expression through the induction of IFN-beta and IL-1 alpha. J. Immunol. 157, 2506–2513.

González-Sanz R, Mata M, Bermejo-Martín J, Álvarez A, Cortijo J, Melero JA, Martínez I (2016): ISG15 is upregulated in respiratory syncytial virus infection and reduces virus growth through protein ISGylation. J. Virol. 90, 3428–3438. https://doi.org/10.1128/JVI.02695-15

Goubau D, Deddouche S, Reise Sousa C (2013): Cytosolic sensing of viruses. Immunity 38, 855–869. https://doi.org/10.1016/j.immuni.2013.05.007

Griffiths C, Drews SJ, Marchant DJ (2017): Respiratory syncytial virus: infection, detection, and new options for prevention and treatment. Clin. Microbiol. Rev. 30, 277–319. https://doi.org/10.1128/CMR.00010-16

Guo X, Liu T, Shi H, Wang J, Ji P, Wang H, Hou Y, Tan RX, Li E (2015): Respiratory syncytial virus infection upregulates NLRC5 and major histocompatibility complex class i expression through RIG-I induction in airway epithelial cells. J. Virol. 89, 7636–7645. https://doi.org/10.1128/JVI.00349-15

Higgins J, Midgley C, Bergh AM, Bell SM, Askham JM, Roberts E, Binns RK, Sharif SM, Bennett C, Glover DM, Woods CG, Morrison EE, Bond J (2010): Human ASPM participates in spindle organisation, spindle orientation and cytokinesis. BMC Cell. Biol. 11, 85-101. https://doi.org/10.1186/1471-2121-11-85

Huang YC, Li Z, Hyseni X, Schmitt M, Devlin RB, Karoly ED, Soukup JM (2008): Identification of gene biomarkers for respiratory syncytial virus infection in a bronchial epithelial cell line. Genomic Med. 2, 113–125. https://doi.org/10.1007/s11568-009-9080-y

Janssen R, Pennings J, Hodemaekers H, Buisman A, van Oosten M, de Rond L, Öztürk K, Dormans J, Kimman T, Hoebee B

(2007): Host transcription profiles upon primary respiratory syncytial virus infection. J. Virol. 81, 5958–5967. https://doi.org/10.1128/JVI.02220-06

Karimian A, Ahmadi Y, Yousefi B (2016): Multiple functions of p21 in cell cycle, apoptosis and transcriptional regulation after DNA damage. DNA Repair (Amst) 42, 63–71. https://doi.org/10.1016/j.dnarep.2016.04.008

Kim TH, Lee HK (2014): Innate immune recognition of respiratory syncytial virus infection. BMB Rep. 47, 184–191. https://doi.org/10.5483/BMBRep.2014.47.4.050

Kirschke CP, Huang L (2003): ZnT7, a novel mammalian zinc transporter, accumulates zinc in the Golgi apparatus. J. Biol. Chem. 278, 4096–4102. https://doi.org/10.1074/jbc.M207644200

Kristiansen H, Gad HH, Eskildsen-Larsen S, Despres P, Hartmann R (2011): The oligoadenylate synthetase family: an ancient protein family with multiple antiviral activities. J. Interferon Cytokine Res. 31, 41–47. https://doi.org/10.1089/jir.2010.0107

Larrañaga C, Ampuero S, Luchsinger V, Carrión F, Aguilar N, Morales P, Palomino MA, Tapia L, Avendaño LF (2009): Impaired immune response in severe human lower tract respiratory infection by respiratory syncytial virus. Pediatr. Infect. Dis. J. 28, 867–873. https://doi.org/10.1097/INF.0b013e3181a3ea71

Lifland AW, Jung J, Alonas E, Zurla C, Crowe JE, Santangelo PJ (2012): Human respiratory syncytial virus nucleoprotein and inclusion bodies antagonize the innate immune response mediated by MDA5 and MAVS. J. Virol. 86, 8245–8258. https://doi.org/10.1128/JVI.00215-12

Ling Z, Tran KC, Teng MN (2009): Human respiratory syncytial virus nonstructural protein NS2 antagonizes the activation of beta interferon transcription by interacting with RIG-I. J. Virol. 83, 3734–3742. https://doi.org/10.1128/JVI.02434-08

Liu P, Jamaluddin M, Li K, Garofalo RP, Casola A, Brasier AR (2007): Retinoic acid-inducible gene i mediates early antiviral response and toll-like receptor 3 expression in respiratory syncytial virus-infected airway epithelial cells. J. Virol. 81, 1401–1411. https://doi.org/10.1128/JVI.01740-06

Livak KJ, Schmittgen TD (2001): Analysis of relative gene expression data using real-time quantitative PCR and the 2-ΔΔCT method. Methods 25, 402–408. https://doi.org/10.1006/meth.2001.1262

Lo MS, Brazas RM, Holtzman MJ (2005): Respiratory syncytial virus nonstructural proteins NS1 and NS2 mediate inhibition of Stat2 expression and alpha/beta interferon responsiveness. J. Virol. 79, 9315–9319. https://doi.org/10.1128/JVI.79.14.9315-9319.2005

Luchsinger V, Ampuero S, Palomino MA, Chnaiderman J, Levican J, Gaggero A, Larrañaga CE (2014): Comparison of virological profiles of respiratory syncytial virus and rhinovirus in acute lower tract respiratory infections in very young Chilean infants, according to their clinical outcome. J. Clin. Virol. 61, 138–144. https://doi.org/10.1016/j.jcv.2014.06.004

Luchsinger V, Piedra PA, Ruiz M, Zunino E, Martínez MA, Machado C, Fasce R, Ulloa MT, Fink MC, Lara P, Avendaño LF (2012): Role of neutralizing antibodies in adults with community-acquired pneumonia by respiratory syncytial virus. Clin Infect Dis. 54, 905–912. https://doi.org/10.1093/cid/cir955

Madhivanan K, Ramadesikan S, Aguilar RC (2015): Role of Ocrl1 in primary cilia assembly. Int. Rev. Cell. Mol. Biol. 317, 331–347. https://doi.org/10.1016/bs.ircmb.2015.02.003

Martínez I, Lombardía L, García-Barreno B, Domínguez O, Melero JA (2007): Distinct gene subsets are induced at different time points after human respiratory syncytial virus infection of A549 cells. J. Gen. Virol. 88, 570–581. https://doi.org/10.1099/vir.0.82187-0

Mayer AK, Muehmer M, Mages J, Gueinzius K, Hess C, Heeg K, Bals R, Lang R,Dalpke AH (2007): Differential recognition of TLR-dependent microbial ligands in human bronchial epithelial cells. J. Immunol. 178, 3134–3142 https://doi.org/10.4049/jimmunol.178.5.3134

McNab F, Mayer-Barber K, Sher A, Wack A, O'Garra A (2015): Type I interferons in infectious disease. Nat. Rev. Immunol. 15, 87–103. https://doi.org/10.1038/nri3787

Mejias A, Dimo B, Suarez NM, Garcia C, Suarez-Arrabal MC, Jartti T, Blankenship D, Jordan-Villegas A, Ardura MI, Xu Z, Banchereau J, Chaussabel D, Ramilo O (2013): Whole blood gene expression profiles to assess pathogenesis and disease severity in infants with respiratory syncytial virus infection. PLoS Med. 10, e1001549. https://doi.org/10.1371/journal.pmed.1001549

Menachery VD, Yount BL Jr, Josset L, Gralinski LE, Scobey T, Agnihothram S, Katze MG, Baric RS (2014): Attenuation and restoration of severe acute respiratory syndrome coronavirus mutant lacking 2'-o-methyltransferase activity. J. Virol. 88, 4251–4264. https://doi.org/10.1128/JVI.03571-13

Moore EC, Barber J, Tripp RA (2008): Respiratory syncytial virus (RSV) attachment and nonstructural proteins modify the type i interferon response associated with suppressor of cytokine signaling (SOCS) proteins and IFN-stimulated gene-15 (ISG15). Virol. J. 5, 116–126. https://doi.org/10.1186/1743-422X-5-116

Morales DJ, Lenschow DJ (2013): The antiviral activities of ISG15. J. Mol. Biol. 425, 4995–5008. https://doi.org/10.1016/j.jmb.2013.09.041

Morales DJ, Monte K, Sun L, Struckhoff JJ, Agapov E, Holtzman MJ, Stappenbeck TS, Lenschow DJ (2015): Novel mode of ISG15-mediated protection against influenza a virus and Sendai virus in mice. J. Virol. 89, 337–349. https://doi.org/10.1128/JVI.02110-14

Mukherjee K, Conway de Macario E, Macario AJ, Brocchieri L (2010): Chaperonin genes on the rise: new divergent classes and intense duplication in human and other vertebrate genomes. BMC Evol Biol. 10, 64–83. https://doi.org/10.1186/1471-2148-10-64

Mukherjee S, Lukacs NW (2013): Innate immune responses to respiratory syncytial virus infection. Curr. Top. Microbiol. Immunol. 372,139–154. https://doi.org/10.1007/978-3-642-38919-1_7

Newland N, Richter A (2008): Agents associated with lung inflammation induce similar responses in NCI-H292 lung epithelial cells. Toxicol. In Vitro 22, 1782–1788. https://doi.org/10.1016/j.tiv.2008.07.009

Parks WC, Wilson CL, López-Boado YS (2004): Matrix metalloproteinases as modulators of inflammation and innate immunity. Nat. Rev. Immunol. 4, 617–629. https://doi.org/10.1038/nri1418

Pérez-Villamil B, Mirasierra M, Vallejo M (2004): The homeoprotein Alx3 contains discrete functional domains and exhibits cell-specific and selective monomeric binding and transactivation. J. Biol. Chem. 279, 38062–38071. https://doi.org/10.1074/jbc.M400800200

Perini AP, Barbosa ML, Botosso VF, de Moraes CT, Gillio AE, Hens N, Stewien KE, Durigon EL (2007): Comparison of HeLa-I, HEp-2 and NCI-H292 cell lines for the isolation of human respiratory syncytial virus (HRSV). J. Virol. Methods 146, 368–371. https://doi.org/10.1016/j.jviromet.2007.07.004

Power D, Santoso N, Dieringer M, Yu J, Huang H, Simpson S, Seth I, Miao H, Zhu J (2015): IFI44 suppresses HIV-1 LTR promoter activity and facilitates its latency. Virology 481, 142–150. https://doi.org/10.1016/j.virol.2015.02.046

Radonić A, Thulke S, Mackay IM, Landt O, Siegert W, Nitsche A (2004): Guideline to reference gene selection for quantitative real-time PCR. Biochem. Biophys. Res. Commun. 313, 856–862. https://doi.org/10.1016/j.bbrc.2003.11.177

Ren J, Liu T, Pang L, Li K, Garofalo RP, Casola A, Bao X (2011): A novel mechanism for the inhibition of interferon regulatory factor-3-dependent gene expression by human respiratory syncytial virus NS1 protein. J. Gen. Virol. 92, 2153–2159. https://doi.org/10.1099/vir.0.032987-0

Russell CD, Stefan A, Unger SA, Walton M, Schwarze J (2017): The human immune response to respiratory syncytial virus infection. Clin. Microbiol. Rev. 30, 481–502. https://doi.org/10.1128/CMR.00090-16

Schmidt ME, Varga SM (2017): Modulation of the host immune response by respiratory syncytial virus proteins. J. Microbiol. 55, 161–171. https://doi.org/10.1007/s12275-017-7045-8

Seidah NG, Prat A (2012): The biology and therapeutic targeting of the proprote in convertases. Nat. Rev. Drug Discov. 11, 367–383. https://doi.org/10.1038/nrd3699

Shahriari S, Gordon J, Ghildyal R (2016): Host cytoskeleton in respiratory syncytial virus assembly and budding. Virol. J. 13, 161-171. https://doi.org/10.1186/s12985-016-0618-z

Singh DP, Fatma N, Kimura A, Chylack LT, Shinohara T (2001): LEDGF binds to heat shock and stress-related element to activate the expression of stress-related genes. Biochem. Biophys. Res. Commun. 283, 943–955. https://doi.org/10.1006/bbrc.2001.4887

Swedan S, Andrews J, Majumdar T, Musiyenko A, Barik S (2011): Multiple functional domains and complexes of the two nonstructural proteins of human respiratory syncytial virus contribute to interferon suppression and cellular location. J. Virol. 85, 10090–10100. https://doi.org/10.1128/JVI.00413-11

Swedan S, Musiyenko A, Barik S (2009): Respiratory syncytial virus nonstructural proteins decrease levels of multiple members of the cellular interferon pathways. J. Virol. 83, 9682–9693. https://doi.org/10.1128/JVI.00715-09

Takaoka A, Yanai H (2006): Interferon signalling network in innate defence. Cell. Microbiol. 8, 907–922. https://doi.org/10.1111/j.1462-5822.2006.00716.x

Tian B, Zhang Y, Luxon BA, Garofalo RP, Casola A, Sinha M, Brasier AR (2002): Identification of NF-κB-dependent gene networks in respiratory syncytial virus-infected cells. J. Virol. 76, 6800–6814. https://doi.org/10.1128/JVI.76.13.6800-6814.2002

Tregoning JS, Schwarze J (2010): Respiratory viral infections in infants: causes, clinical symptoms, virology, and immunology. Clin. Microbiol. Rev. 23, 74–98. https://doi.org/10.1128/CMR.00032-09

Turner T, Kopp B, Paul G, Landgrave L, Hayes D, Thompson R (2014): Respiratory syncytial virus: current and emerging treatment options. Clinicoecon. Outcomes Res. 6, 217–225. https://doi.org/10.2147/CEOR.S60710

Walker MG, Volkmuth W (2002): Cell adhesion and matrix remodeling genes identified by co-expression analysis. Gene Funct. Dis. 3, 109–112. https://doi.org/10.1002/gnfd.200290000

Welliver TP, Reed JL, Welliver RC (2008): Respiratory syncytial virus and influenza virus infections: observations from tissues of fatal infant cases. Pediatr. Infect. Dis. J. 27, S92–S96. https://doi.org/10.1097/INF.0b013e318168b706

Wu W, Tran KC, Teng MN, Heesom KJ, Matthews DA, Barr JN, Hiscox JA (2012): The interactome of the human respiratory syncytial virus NS1 protein highlights multiple effects on host cell biology. J. Virol. 86, 7777–7789. https://doi.org/10.1128/JVI.00460-12

Yagi A, Hasegawa Y, Xiao H, Haneda M, Kojima E, Nishikimi A, Hasegawa T, Shimokata K, Isobe K (2003): GADD34 induces p53 phosphorylation and p21/WAF1 transcription. J. Cell. Biochem. 90, 1242–1249. https://doi.org/10.1002/jcb.10711

Zhang Y, Jamaluddin M, Wang S, Tian B, Garofalo RP, Casola A, Brasier AR (2003): Ribavirin treatment up-regulates antiviral gene expression via the interferon-stimulated response element in respiratory syncytial virus-infected epithelial cells. J. Virol. 77, 5933–5947. https://doi.org/10.1128/JVI.77.10.5933-5947.2003

Zhang Y, Luxon BA, Casola A, Garofalo RP, Jamaluddin M, Brasier AR (2001): Expression of respiratory syncytial virus-induced chemokine gene networks in lower airway epithelial cells revealed by cDNA microarrays. J. Virol. 75, 9044–9058. https://doi.org/10.1128/JVI.75.19.9044-9058.2001

Zhao C, Collins MN, Hsiang TY, Krug RM (2013): Interferon-induced ISG15 pathway: an ongoing virus-host battle. Trends Microbiol. 21, 181–186. https://doi.org/10.1016/j.tim.2013.01.005

Zhu J, Ghosh A, Sarkar SN (2015): OASL-a new player in controlling antiviral innate immunity. Curr. Opin. Virol. 12, 15–19. https://doi.org/10.1016/j.coviro.2015.01.010

Acta virologica **62**: 310 – 325, 2018 doi:10.4149/av_2018_225

Supplementary information

Time-course of transcriptome response to respiratory syncytial virus infection in lung epithelium cells

S. AMPUERO[1], R. ANDAUR[1], M. MILANO[1], M. MORENO[2], L. LIZAMA[1], C. LARRAÑAGA[1], U. URZÚA[3]

[1]Virology Program, Institute of Biomedical Sciences, Faculty of Medicine, University of Chile; Postal address 8380453, Independencia 1027, Independencia, Santiago, Chile; [2]Laboratory of Oncology and Molecular Genetics, Coloproctology Unit, Clinica Las Condes, Santiago, Chile; Postal address 7591046, Santiago, Chile; [3]Department of Basic and Clinical Oncology, Faculty of Medicine, University of Chile, Postal adress 8380453, Santiago, Chile

Received December 27, 2017; revised February 2, 2018; accepted July 12, 2018

Supplementary Table S1. List of 330 differentially expressed genes after RSV infection (p value <0.01)

Gene symbol	Gene name	Fc				
		0 hpi	24 hpi	48 hpi	72 hpi	96 hpi
AARS	alanyl-tRNA synthetase	-0.39	-0,61	0,73	0,40	-1,77
ABCC8	ATP-binding cassette, sub-family C (CFTR/MRP), member 8	0.68	0,95	-1,09	1,13	1,16
ACACA	acetyl-CoA carboxylase alpha	0.16	-0,59	-0,84	-0,88	1,23
ADAM8	ADAM metallopeptidase domain 8	-0.13	0,76	0,80	0,67	-2,81
ADAR	adenosine deaminase, RNA-specific	0.29	0,91	1,17	0,55	-1,67
AHNAK	AHNAK nucleoprotein	-0.37	-1,64	-1,42	0,61	2,51
AHR	aryl hydrocarbon receptor	-0.05	-0,21	0,91	1,01	-2,85
ALDH1A3	aldehyde dehydrogenase 1 family, member A3	0.28	1,11	-0,21	0,95	-1,51
ALX3	ALX homeobox 3	0.17	-0,02	4,08	0,15	-0,54
ANK3	ankyrin 3, node of Ranvier	-0.06	-1,00	0,53	-0,29	1,21
ANKRD36	Ankyrin repeat domain 36	0.26	0,32	-1,24	1,13	1,31
ANKRD36B	ankyrin repeat domain 36B	0.59	0,64	-1,30	0,21	1,66
ANXA8L1	annexin A8-like 1	-0.10	-0,30	-1,55	-0,12	2,82
AQP3	aquaporin 3 (Gill blood group)	0.65	-0,10	1,19	0,00	-1,60
AREG	amphiregulin	0.77	1,14	0,81	2,13	-3,37
ARHGDIB	Rho GDP dissociation inhibitor (GDI) beta	0.16	-0,62	0,62	-0,72	2,03
ARL6IP5	ADP-ribosylation-like factor 6 interacting protein 5	0.06	-0,10	-1,14	-1,11	1,38
ARRDC3	arrestin domain containing 3	0.20	0,61	0,37	1,18	-1,69
ASAM	adipocyte-specific adhesion molecule	0.46	-0,27	0,08	0,19	-1,57
ASNS	asparagine synthetase (glutamine-hydrolyzing)	-0.49	-0,05	0,67	0,25	-2,62
ASPM	asp (abnormal spindle) homolog, microcephaly associated (Drosophila)	0.25	-4,26	0,18	-0,06	3,14
ATF3	activating transcription factor 3	-0.23	0,74	0,04	2,24	-0,90
ATOH8	atonal homolog 8 (Drosophila)	-0.20	-2,03	-0,26	-1,72	4,18
B2M	Beta-2-microglobulin	0.02	1,48	1,59	1,20	-2,15
BCAM	basal cell adhesion molecule (Lutheran blood group)	-0.11	-0,83	-0,69	-0,93	1,39
BCAR3	breast cancer anti-estrogen resistance 3	-0.83	-0,05	-0,48	1,74	-0,53
BCL2L1	BCL2-like 1	-0.29	-0,94	0,76	0,66	-2,11
BIRC3	baculoviral IAP repeat-containing 3	0.18	-0,16	-0,48	-0,03	-3,32
BLOC1S1	biogenesis of lysosomal organelles complex-1, subunit 1	0.03	-0,23	-0,15	-2,46	0,09

Gene symbol	Gene name	Fc				
		0 hpi	24 hpi	48 hpi	72 hpi	96 hpi
BTN2A1	Butyrophilin, subfamily 2, member A1	-0.55	1,97	0,14	1,73	-1,48
CARS	cysteinyl-tRNA synthetase	0.20	-0,06	-0,30	1,74	-2,69
CCL20	chemokine (C-C motif) ligand 20	-0.22	0,30	0,93	0,32	-2,36
CCL4L2	chemokine (C-C motif) ligand 4-like 2	0.38	0,48	3,66	-0,18	-2,37
CCNA2	cyclin A2	0.16	-0,50	-0,59	-0,14	2,55
CCNB1	cyclin B1	-0.25	-0,26	-0,87	-0,35	2,24
CCNB2	cyclin B2	-0.05	-0,23	-0,40	-0,65	2,03
CCND1	cyclin D1	-0.12	0,71	0,13	1,27	-2,05
CCT6A	chaperonin containing TCP1, subunit 6A (zeta 1)	-0.04	-0,28	0,07	-3,11	0,07
CD55	CD55 molecule, decay accelerating factor for complement (Cromer blood group)	0.46	1,53	2,04	0,80	-2,17
CD59	CD59 molecule, complement regulatory protein	-0.04	0,13	-1,78	0,04	2,80
CDCP1	CUB domain containing protein 1	0.33	0,90	1,27	0,49	-1,76
CDH23	cadherin-related 23	0.51	1,56	-1,07	0,02	0,50
CDK1	cyclin-dependent kinase 1	-0.22	-0,44	0,02	-0,59	3,19
CDKN1A	cyclin-dependent kinase inhibitor 1A (p21, Cip1)	-0.40	-0,29	0,44	2,02	-2,08
CEBPB	CCAAT/enhancer binding protein (C/EBP), beta	0.02	-0,48	0,77	0,77	-1,52
CEBPG	CCAAT/enhancer binding protein (C/EBP), gamma	0.29	0,23	-0,04	1,23	-1,74
CENPF	centromere protein F	0.42	-0,02	0,00	-0,33	2,66
CFB	complement factor B	0.26	0,49	1,00	1,06	-1,39
CFI	complement factor I	0.08	-0,25	-0,01	-0,59	2,46
CHMP5	chromatin modifying protein 5	-0.58	0,64	0,84	0,22	-1,17
CKS2	CDC28 protein kinase regulatory subunit 2	0.23	-0,46	0,96	-0,51	2,34
CNOT1	CCR4-NOT transcription complex, subunit 1	-0.16	0,29	0,46	-2,46	-0,26
COL12A1	collagen, type XII, alpha 1	-0.02	-0,35	-0,58	-0,56	1,98
COL5A1	collagen, type V, alpha 1	-0.02	0,03	-0,75	-0,50	2,62
COX7B	cytochrome c oxidase subunit VIIb (COX7B), nuclear gene encoding mitochondrial protein	0.90	-0,65	-1,01	-0,55	0,78
CPSF1	cleavage and polyadenylation specific factor 1	0.11	0,46	2,77	0,01	-0,76
CSNK1A1	casein kinase 1, alpha 1	-0.95	-0,13	0,76	1,00	-1,32
CTSC	cathepsin C	-0.21	-0,13	0,82	-1,24	0,60
CXCL1	chemokine (C-X-C motif) ligand 1	-0.16	0,40	1,50	0,54	-2,04
CXCL11	chemokine (C-X-C motif) ligand 11	0.25	3,68	1,08	2,39	-3,82
CXCL3	chemokine (C-X-C motif) ligand 3	0.22	0,67	1,51	1,17	-1,95
CYBRD1	cytochrome b reductase 1	0.44	-0,47	-0,53	0,16	2,44
DDIT3	DNA-damage-inducible transcript 3	0.38	0,11	1,15	3,33	-1,71
DDX58	DEAD (Asp-Glu-Ala-Asp) box polypeptide 58	0.07	1,38	0,47	1,54	-4,31
DDX60	DEAD (Asp-Glu-Ala-Asp) box polypeptide 60	0.27	0,95	1,01	3,21	-2,61
DDX60L	DEAD (Asp-Glu-Ala-Asp) box polypeptide 60-like	0.41	1,55	1,64	1,34	-3,61
DEFB1	defensin, beta 1 (DEFB1)	0.05	0,39	-0,73	-0,79	3,20
DNAJC2	DNAJC2 -- DnaJ (Hsp40) homolog, subfamily C, member 2	0.60	-1,86	-0,37	0,15	-0,63
DNAJC25-GNG10	DNAJC25-GNG10 readthrough	-0.29	-0,99	-0,41	-1,51	0,92
DTX3L	deltex 3-like (Drosophila)	-0.07	0,77	0,62	1,00	-2,42
DUSP4	dual specificity phosphatase 4	0.27	0,13	1,09	-0,37	-4,02
DUSP6	dual specificity phosphatase 6	-0.17	0,91	0,08	-0,12	-2,52
EDARADD	EDAR-associated death domain	0.88	-0,08	-1,30	-1,71	0,24
EFEMP1	EGF-containing fibulin-like extracellular matrix protein 1	-0.19	-0,60	-0,06	-0,50	3,17
EGFL8	EGF-like-domain, multiple 8	0.64	0,68	2,31	-0,27	-1,11
EIF1	eukaryotic translation initiation factor 1	-0.31	-0,24	0,75	-0,02	-1,98
EIF2AK2	eukaryotic translation initiation factor 2-alpha kinase 2	0.47	0,14	1,00	0,65	-2,49
EIF2C2	eukaryotic translation initiation factor 2C	-0.74	0,40	1,62	1,68	-0,96
EIF3L	eukaryotic translation initiation factor 3, subunit L	0.07	-1,07	-0,26	-0,97	1,43
EMP2	epithelial membrane protein 2	0.83	0,02	-0,64	-0,33	2,47

Gene symbol	Gene name	Fc				
		0 hpi	24 hpi	48 hpi	72 hpi	96 hpi
EPHX1	epoxide hydrolase 1, microsomal (xenobiotic)	0.50	-0,37	-1,00	-0,82	1,52
ERMP1	endoplasmic reticulum metallopeptidase 1	0.07	-0,77	-0,70	-0,52	1,70
ETV4	ets variant 4	0.91	-1,29	-0,23	0,72	-1,85
F3	coagulation factor III (thromboplastin, tissue factor)	0.34	1,78	1,44	1,66	-1,79
FAM3C	family with sequence similarity 3, member C	-0.12	0,82	0,79	1,29	-2,02
FN1	fibronectin 1	-0.01	2,07	-0,61	2,49	0,30
FOLR1	folate receptor 1	-0.17	-0,48	-0,72	-0,86	2,43
FOSL1	FOS-like antigen 1	0.36	0,59	0,33	1,37	-2,09
FST	follistatin	-0.10	1,36	2,66	2,02	-6,89
GARS	glycyl-tRNA synthetase	0.51	-0,20	0,24	0,52	-2,02
GBP1	guanylate binding protein 1, interferon-inducible, 67kDa	-0.08	1,60	2,07	0,41	-2,87
GBP3	guanylate binding protein 3	-0.27	0,62	0,66	1,12	-1,57
GCNT3	glucosaminyl (N-acetyl) transferase 3, mucin type	-0.13	0,25	0,29	0,86	-2,22
GDF15	growth differentiation factor 15	-0.10	0,16	0,23	0,42	-4,37
GLA	galactosidase, alpha	-0.96	-0,20	1,50	-0,12	1,20
GMNN	geminin, DNA replication inhibitor	0.37	0,34	-0,05	-0,38	1,88
GPR109A	G protein-coupled receptor 109A	-0.09	-0,46	-1,00	0,02	3,62
GPR109B	G protein-coupled receptor 109B	0.03	-0,53	-1,29	-0,27	3,18
GSG1	germ cell associated 1	-0.91	0,14	-0,96	0,19	2,49
GTPBP2	GTP binding protein 2	-0.59	0,73	0,25	1,26	-2,44
H19	imprinted maternally expressed transcript	-0.16	-0,55	-0,28	-0,42	2,82
H1F0	H1 histone family, member 0	0.31	-0,28	2,70	1,12	-2,73
HADHB	hydroxyacyl-CoA dehydrogenase, beta subunit	0.39	-0,40	-1,39	-0,16	1,36
HBEGF	heparin-binding EGF-like growth factor	-0.66	1,68	1,95	1,81	-3,87
HDAC9	histone deacetylase 9	0.57	0,07	0,11	0,96	-2,48
HERC5	hect domain and RLD 5	-0.01	2,83	0,61	2,05	-3,15
HERC6	hect domain and RLD 6	0.74	0,91	0,76	1,12	-3,44
HIST1H1B	histone cluster 1, H1b	-0.42	0,46	-1,12	-0,42	3,51
HIST1H2AJ	histone cluster 1, H2aj	-0.54	-0,20	-0,45	0,31	2,09
HIST1H3I	histone cluster 1, H3i	-0.55	0,23	-0,59	0,17	1,64
HIST1H4C	histone cluster 1, H4c	0.33	-0,43	-0,92	-0,13	2,54
HLA-A	major histocompatibility complex, class I, A	0.17	2,14	3,80	3,42	-4,62
hLA-B	major histocompatibility complex, class I, B	-0.35	2,09	2,73	3,02	-4,19
HLA-C	major histocompatibility complex, class I, C	-0.26	1,68	3,06	2,16	-3,80
HLA-E	major histocompatibility complex, class I, E	0.01	1,63	2,93	2,62	-3,28
HLA-F	major histocompatibility complex, class I, F	-0.28	1,67	2,25	1,97	-3,48
HLA-G	major histocompatibility complex, class I, G	-0.03	1,13	1,54	2,29	-3,29
HLA-H	major histocompatibility complex, class I, H	-0.17	1,56	2,67	1,19	-3,66
HMGA1	high mobility group AT-hook 1	0.06	0,12	-0,15	-0,03	-0,42
HMGB2	high-mobility group box 2	0.83	-0,38	0,29	-0,11	2,21
HSPB8	heat shock 22kDa protein 8	-0.14	-0,44	-0,92	0,21	3,02
HTRA2	HtrA serine peptidase 2	-0.09	0,08	1,72	-0,10	-0,49
ID1	inhibitor of DNA binding 1	-0.13	-0,17	-1,41	-0,42	2,87
ID3	inhibitor of DNA binding 3	-0.19	-0,82	-0,37	-0,56	3,21
IER3	immediate early response 3	0.03	1,64	1,20	0,94	-2,83
IER5	immediate early response 5	0.40	0,36	-0,03	1,10	-1,12
IFI35	interferon-induced protein 35	0.13	1,93	0,48	0,93	-2,93
IFI44	interferon-induced protein 44	0.08	4,74	1,61	3,41	-5,55
IFI44L	interferon-induced protein 44-like	-0.06	0,41	1,21	0,21	-4,17
IFI6	interferon, alpha-inducible protein 6	-0.25	0,55	0,66	0,18	-3,30
IFIH1	interferon induced with helicase C domain 1	0.26	2,20	1,67	2,33	-4,14
IFIT1	interferon-induced protein with tetratricopeptide repeats 1	-0.36	6,13	2,54	2,73	-6,42
IFIT3	interferon-induced protein with tetratricopeptide repeats 3	0.12	1,72	0,31	2,30	-3,27

Gene symbol	Gene name	Fc				
		0 hpi	24 hpi	48 hpi	72 hpi	96 hpi
IFIT5	interferon-induced protein with tetratricopeptide repeats 5	-0.26	1,15	-0,98	0,97	-2,46
IFITM1	interferon induced transmembrane protein 1 (9-27) (IFITM1)	-0.11	1,86	1,78	1,32	-2,86
IFRD1	interferon-related developmental regulator 1 (IFRD1), transcript variant 2	0.09	0,60	0,10	0,86	-1,76
IGFBP1	insulin-like growth factor binding protein 1 (IGFBP1).	0.57	1,54	-1,65	-0,19	0,03
IGFBP3	insulin-like growth factor binding protein 3 (IGFBP3), transcript variant 2	0.13	0,39	1,45	0,66	-1,84
IL1A	interleukin 1, alpha (IL1A)	0.53	1,28	0,17	0,79	-1,79
IL1RL1	interleukin 1 receptor-like 1 (IL1RL1), transcript variant 1	0.37	1,49	-0,06	-0,49	-0,77
IL23A	interleukin 23, alpha subunit p19	0.20	1,49	0,09	1,48	-1,56
IL24	interleukin 24 (IL24), transcript variant 5	-0.14	1,03	1,49	0,35	-3,69
IL6	interleukin 6 (interferon, beta 2) (IL6)	0.47	1,08	0,84	1,46	-2,78
IL8	interleukin 8	0.11	1,13	1,40	1,31	-3,00
INHA	inhibin, alpha	-0.54	-2,11	0,57	-0,09	2,29
IRF7	interferon regulatory factor 7	-0.62	1,86	0,31	1,50	-1,77
IRF9	interferon regulatory factor 9	0.28	1,66	0,70	2,18	-3,44
ISG15	ISG15 ubiquitin-like modifier	-0.54	2,35	1,45	3,42	-6,86
ISG20	interferon stimulated exonuclease gene 20kDa	0.30	2,42	0,60	3,50	-3,51
ISPD	isoprenoid synthase domain containing	0.10	-0,23	2,33	-0,27	-0,26
ITGB1	integrin, beta 1	0.51	1,11	0,64	0,18	-1,34
KCNJ1	potassium inwardly-rectifying channel, subfamily J, member 1	0.10	0,66	1,69	0,94	-2,87
KIAA0182	KIAA0182	-0.57	0,01	1,84	-0,23	-0,39
KIF20A	kinesin family member 20A	0.81	-0,53	-0,97	-0,67	0,87
KLF5	Kruppel-like factor 5 (intestinal)	0.18	0,54	1,01	0,87	-1,37
KPNA2	karyopherin alpha 2 (importin alpha 1)	0.36	0,06	-0,06	-0,09	2,31
KRTAP4-6	keratin associated protein 4-6	0.41	0,50	-1,59	0,17	-0,67
LAMC2	laminin, gamma 2	0.20	4,02	0,11	2,28	-1,36
LAMP3	lysosomal-associated membrane protein 3	0.38	3,03	0,97	1,08	-3,22
LAP3	leucine aminopeptidase 3	0.11	0,70	0,85	0,14	-2,14
LCN2	lipocalin 2	-0.09	0,56	2,17	0,68	-2,67
LDLR	low density lipoprotein receptor	-0.39	0,24	0,83	1,06	-2,08
LGALS3BP	lectin, galactoside-binding, soluble, 3 binding protein	-0.19	0,35	1,44	0,44	-2,12
LGALS9	lectin, galactoside-binding, soluble, 9	0.12	1,37	0,41	0,76	-2,55
LIF	leukemia inhibitory factor (cholinergic differentiation factor)	0.17	0,59	0,36	1,14	-1,81
LRP1	low density lipoprotein receptor-related protein 1	-0.20	-0,60	-0,95	-0,13	1,54
MAFK	v-maf musculoaponeurotic fibrosarcoma oncogene homolog K	-0.09	0,30	0,70	1,11	-1,81
MAP2	microtubule-associated protein 2	-0.60	-1,20	0,26	1,12	1,30
MAPK8	mitogen-activated protein kinase 8	0.75	-0,39	-0,58	-0,35	1,41
MARS	methionyl-tRNA synthetase	0.15	-0,28	2,70	1,12	-2,70
MBOAT7	membrane bound O-acyltransferase domain containing 7	0.59	-0,09	-1,31	-0,20	1,19
MDK	midkine (neurite growth-promoting factor 2)	0.17	0,52	1,26	0,40	-1,36
MDM2	Mdm2 p53 binding protein homolog	-0.05	-0,18	0,79	0,92	-2,05
METTL7A	methyltransferase like 7A	0.41	-0,59	-0,07	-0,80	2,29
MFF	mitochondrial fission factor	0.16	-0,90	0,75	-0,49	1,23
MGST1	microsomal glutathione S-transferase 1	0.35	-0,19	-1,24	-0,88	1,38
MICAL2	microtubule associated monoxygenase, calponin and LIM domain containing 2	0.63	0,91	0,81	0,70	-2,52
MLKL	mixed lineage kinase domain-like	-0.68	-0,07	0,93	0,55	-1,68
MMP1	matrix metallopeptidase 1 (interstitial collagenase)	0.72	3,38	0,66	0,83	-3,20
MOCOS	molybdenum cofactor sulfurase	0.04	-0,18	0,58	1,31	-1,97
MSH6	mutS homolog 6	0.11	0,10	-0,03	-1,50	0,83
MST1R	MST1R – macrophage stimulating 1 receptor (c-met-related tyrosine kinase)	-0.42	1,42	-0,15	0,33	-1,36
MT1DP	metallothionein 1D (pseudogene)	-0.29	-0,35	-1,86	-0,91	1,75
MT1E	metallothionein 1E	0.31	-0,72	-0,68	-0,51	2,28

Gene symbol	Gene name	Fc				
		0 hpi	24 hpi	48 hpi	72 hpi	96 hpi
MT1M	metallothionein 1M	0.10	-0,83	-0,50	-1,23	2,50
MTHFD2	methylenetetrahydrofolate dehydrogenase (NADP+ dependent) 2, methenyltetrahydrofolate cyclohydrolase	0.02	0,49	0,86	0,69	-2,65
MT-TR	mitochondrially encoded tRNA arginine	0.38	0,30	2,41	0,72	-3,26
MTX1	metaxin 1	-0.16	0,16	3,12	-0,13	-2,99
MX1	myxovirus (influenza virus) resistance 1	-0.07	4,55	3,36	1,70	-6,31
MX2	myxovirus (influenza virus) resistance 2	-0.61	2,24	0,98	1,26	-4,58
MXRA5	matrix-remodelling associated 5	0.04	-1,32	-1,01	-1,58	3,44
MYD88	myeloid differentiation primary response gene (88)	0.86	-0,73	0,52	0,92	-1,73
MYO9A	myosin IXA	-0.06	-0,20	-2,38	0,22	0,82
NAMPT	nicotinamide phosphoribosyltransferase	0.15	0,37	1,12	0,92	-2,56
NCAPG2	non-SMC condensin II complex, subunit G2	-0.19	-0,06	-1,11	0,01	2,38
NMI	N-myc (and STAT) interactor	0.25	1,09	0,15	0,41	-2,85
NNMT	nicotinamide N-methyltransferase	0.10	-1,46	-0,36	-0,58	1,83
NNT	nicotinamide nucleotide transhydrogenase	-0.14	-1,00	0,14	-0,67	1,43
NOTCH3	notch 3	0.11	-1,29	-0,66	0,09	2,32
NPC2	Niemann-Pick disease, type C2	0.01	-0,01	-0,82	-0,26	2,01
NT5DC2	5'-nucleotidase domain containing 2	-0.71	-0,09	-0,55	-0,25	1,41
NUSAP1	nucleolar and spindle associated protein 1	0.25	0,08	-0,23	-0,35	3,39
OAS1	2',5'-oligoadenylate synthetase 1	-0.41	3,41	2,43	2,79	-5,90
OAS2	2'-5'-oligoadenylate synthetase 2, 69/71 kDa	-0.05	2,56	3,07	1,09	-6,96
OAS3	2'-5'-oligoadenylate synthetase 3, 100 kDa	0.27	2,11	1,93	1,27	-4,54
OASL	2'-5'-oligoadenylate synthetase-like	0.20	2,37	0,63	2,16	-5,11
OCRL	oculocerebrorenal syndrome of Lowe	-0.14	-0,10	-2,50	-0,32	-0,68
OLR1	oxidized low density lipoprotein (lectin-like) receptor 1	0.37	-0,99	-1,21	-0,40	2,30
OSTM1	osteopetrosis associated transmembrane protein 1	0.80	-0,03	1,78	0,14	-1,34
PARP14	poly (ADP-ribose) polymerase family, member 14	0.09	0,33	0,48	1,84	-2,27
PARP9	poly (ADP-ribose) polymerase family, member 9	-0.12	1,73	-0,16	0,68	-2,52
PATL1	protein associated with topoisomerase II homolog 1	-0.20	0,47	0,41	0,43	-2,19
PCSK9	proprotein convertase subtilisin/kexin type 9	0.00	-0,99	-0,22	1,85	-1,14
PDE4B	phosphodiesterase 4B, cAMP-specific	-0.46	-1,07	0,65	0,59	-2,24
PER2	PER2 – period homolog 2	-0.26	0,10	1,81	0,10	-0,78
PERP	PERP – PERP, TP53 apoptosis effector	-0.13	-0,37	-0,99	0,00	1,29
PHLDA1	PHLDA1 – pleckstrin homology-like domain, family A, member 1	0.23	0,42	0,31	1,31	-2,22
PHTF2	putative homeodomain transcription factor 2	-0.26	0,58	-0,61	-0,70	3,58
PLAUR	plasminogen activator, urokinase receptor	-0.42	1,37	-0,07	1,49	-1,76
PLSCR1	phospholipid scramblase 1 (PLSCR1).	0.96	1,01	0,85	0,81	-3,16
PLUNC	palate, lung and nasal epithelium associated	0.21	-0,19	2,70	-0,16	-5,69
PMAIP1	phorbol-12-myristate-13-acetate-induced protein 1	0.25	1,11	1,40	3,17	-3,17
PPM1K	protein phosphatase, Mg2+/Mn2+ dependent, 1K	0.40	0,60	-0,98	0,34	-1,76
PPP1R15A	protein phosphatase 1, regulatory (inhibitor) subunit 15A	-0.17	0,86	-0,35	3,02	-2,71
PRC1	protein regulator of cytokinesis 1	-0.40	-0,43	0,64	-0,12	1,69
PRIC285	peroxisomal proliferator-activated receptor A interacting complex 285	-0.20	2,59	-0,21	1,37	-4,12
PRKAR2B	protein kinase, cAMP-dependent, regulatory, type II, beta	-0.21	0,44	0,39	0,67	-1,65
PRKD2	protein kinase D2	0.12	1,02	-1,27	0,47	-1,29
PROM2	prominin 2	-0.15	-0,64	-0,51	-0,30	1,93
PRSS23	protease, serine, 23	0.01	0,14	-0,94	1,27	1,43
PSIP1	PC4 and SFRS1 interacting protein 1	0.74	-0,10	-1,04	-3,30	1,49
PSMB8	proteasome (prosome, macropain) subunit, beta type, 8	0.26	1,03	0,44	0,04	-1,45
PSMB9	proteasome (prosome, macropain) subunit, beta type, 9	-0.01	1,47	-0,07	1,42	-1,65
PTGS2	prostaglandin-endoperoxide synthase 2	0.37	0,76	1,80	0,97	-3,28
PTPRF	protein tyrosine phosphatase, receptor type, F	0.16	-0,38	-1,05	-0,21	2,32
RAB31	RAB31, member RAS oncogene family	0.15	0,40	0,60	0,87	-1,62

Gene symbol	Gene name	Fc				
		0 hpi	24 hpi	48 hpi	72 hpi	96 hpi
RAB3IL1	RAB3A interacting protein (rabin3)-like 1	0.26	0,63	2,32	0,21	-1,40
RAP1GAP2	RAP1 GTPase activating protein 2	0.47	1,18	-0,64	0,61	-5,28
RCN2	reticulocalbin 2	0.15	0,06	-0,26	-2,04	0,70
REC8	REC8 homolog	0.65	2,08	0,67	0,91	-1,60
RHOV	ras homolog gene family, member V	0.12	-0,24	-1,41	-0,47	1,28
RICTOR	RPTOR independent companion of MTOR, complex 2	0.83	0,67	1,84	0,86	-2,53
RNF19B	ring finger protein 19B	0.23	0,54	0,43	0,03	-1,83
RPA1	replication protein A1, 70 kDa	0.53	-0,78	0,59	-0,09	1,51
RPL7	ribosomal protein L7	-0.10	-0,75	-0,83	-1,71	0,75
RRM1	ribonucleotide reductase M1	0.22	-0,38	-0,75	-0,82	2,19
S100A8	S100 calcium binding protein A8	0.04	0,52	1,88	0,04	-3,26
S100A9	S100 calcium binding protein A9	-0.08	0,01	2,27	-0,31	-1,63
SAMD9L	sterile alpha motif domain containing 9-like	0.43	1,47	-0,86	-0,53	-2,21
SAMHD1	SAM domain and HD domain 1	-0.60	1,28	0,21	1,23	-3,23
SAV1	salvador homolog 1	-0.20	0,20	0,41	0,92	-2,02
SCD5	stearoyl-CoA desaturase 5	-0.18	0,11	-1,34	-0,24	1,04
SCPEP1	serine carboxypeptidase 1	-0.02	-0,43	0,38	-0,19	2,29
SERPINB4	serpin peptidase inhibitor, clade B (ovalbumin), member 4	0.00	-0,50	0,05	-2,37	0,03
SHMT2	serine hydroxymethyltransferase 2	0.12	-0,56	1,00	-0,18	-1,52
SHROOM3	shroom family member 3	-0.17	0,02	0,29	0,90	-1,39
SLC16A2	solute carrier family 16, member 2	0.28	-0,38	-0,62	0,10	2,36
SLC30A7	solute carrier family 30, member 7	-0.22	-0,18	-0,22	3,08	-1,46
SLC6A14	solute carrier family 6 , member 14	0.76	0,06	0,53	0,37	-2,17
SLC6A9	solute carrier family 6 , member 9	-0.13	0,19	0,03	0,37	-2,37
SMOX	spermine oxidase	-0.55	-0,13	0,33	0,20	-1,87
SNCG	synuclein, gamma	0.20	-1,16	-0,86	0,06	2,55
SOX9	SRY (sex determining region Y)-box 9	-0.28	0,96	-0,25	2,00	-2,37
SP110	SP110 nuclear body protein	-0.26	0,78	0,75	0,59	-2,22
SPAG5	sperm associated antigen 5	0.36	-0,12	-0,71	0,06	2,31
SQRDL	sulfide quinone reductase-like	0.17	0,60	-0,02	0,88	-1,46
ST6GALNAC2	ST6 (alpha-N-acetyl-neuraminyl-2,3-beta-galactosyl-1, 3)-N-acetylgalactosaminide alpha-2,6-sialyltransferase 2	0.50	-0,33	0,76	-0,07	2,16
STAG3L3	stromal antigen 3-like 3	-0.70	0,13	-0,68	-1,25	1,17
STAT1	signal transducer and activator of transcription 1, 91 kDa	-0.10	2,40	1,59	0,71	-3,83
STAT2	signal transducer and activator of transcription 2, 113 kDa	0.12	1,39	1,68	0,84	-1,89
STC1	Stanniocalcin 1	0.19	1,70	1,35	0,86	-5,39
STC2	stanniocalcin 2	0.55	1,33	1,36	1,01	-2,75
STK40	serine/threonine kinase 40	0.16	0,21	0,32	0,35	-1,61
STMN1	stathmin 1	-0.32	0,15	-0,55	-0,32	2,59
SYNE2	spectrin repeat containing, nuclear envelope 2	-0.25	-0,02	-0,78	0,03	1,80
SYNPO	synaptopodin	0.05	-0,95	-0,93	-0,18	1,58
TACC2	transforming, acidic coiled-coil containing protein 2	-0.03	-0,89	0,03	-0,12	2,19
TAP1	transporter 1, ATP-binding cassette, sub-family B	0.11	1,90	0,76	5,68	-2,68
TARS	threonyl-tRNA synthetase	0.30	0,04	1,16	0,44	-1,16
TBC1D7	TBC1 domain family, member 7	0.05	-1,72	0,72	-0,97	-0,31
TCEB3B	transcription elongation factor B polypeptide 3B	-0.09	0,58	1,06	1,04	-2,32
TCF7	transcription factor 7 (T-cell specific, HMG-box)	0.27	0,25	2,10	0,67	-2,40
TCTN1	tectonic family member 1	-0.46	-1,65	-0,51	0,88	0,70
TECR	trans-2,3-enoyl-CoA reductase	0.24	-0,93	-0,97	-0,50	1,31
TFPI2	tissue factor pathway inhibitor 2	-0.01	0,47	0,18	2,00	-1,46
TGFB2	transforming growth factor, beta 2	-0.24	0,32	0,52	0,93	-1,81
TGIF1	TGFB-induced factor homeobox 1	0.12	-0,14	1,46	1,03	-1,87
TK1	thymidine kinase 1	0.32	-0,61	-0,58	-0,09	2,66

Gene symbol	Gene name	Fc				
		0 hpi	**24 hpi**	**48 hpi**	**72 hpi**	**96 hpi**
TLN1	talin 1	-0.40	-0,50	-0,78	-0,27	1,39
TLR9	toll-like receptor 9	-0.88	-0,20	-1,54	-0,55	1,29
TMC5	transmembrane channel-like 5	0.21	0,97	-0,35	0,62	-3,24
TMEM132A	transmembrane protein 132A	0.14	0,31	-0,86	1,49	-1,52
TMEM27	transmembrane protein 27	0.78	0,67	-0,08	0,86	-1,65
TNFAIP3	tumor necrosis factor, alpha-induced protein 3	-0.65	0,53	1,29	1,69	-1,62
TOP1	topoisomerase (DNA) I	0.59	0,34	0,71	0,95	-1,22
TOP2A	topoisomerase (DNA) II alpha 170 kDa	0.09	-0,64	-0,57	-0,71	3,93
TPBG	trophoblast glycoprotein	-0.10	0,46	1,23	0,59	-1,62
TPX2	TPX2, microtubule-associated, homolog (Xenopus laevis)	0.14	-0,40	-0,26	-0,59	3,20
TRAM1	translocation associated membrane protein 1	-0.03	0,15	-1,20	-0,40	1,32
TRAPPC1	trafficking protein particle complex 1	-0.31	0,06	-0,14	-1,21	1,32
TRIB3	tribbles homolog 3 (Drosophila)	0.12	0,47	0,47	1,24	-1,28
TRIM14	tripartite motif-containing 14	-0.06	0,33	0,32	0,37	-2,18
TRIM21	tripartite motif-containing 21	0.54	1,24	1,40	0,82	-1,99
TRIM22	tripartite motif-containing 22	-0.04	1,60	-0,35	0,14	-2,44
TRIM29	tripartite motif-containing 29	-0.08	-1,30	-1,57	-0,75	1,66
TRIM5	tripartite motif-containing 5	0.33	0,49	0,69	0,17	-1,56
TSC22D1	TSC22 domain family, member 1	0.20	0,36	0,80	0,85	-2,02
TXNIP	thioredoxin interacting protein	0.35	0,28	0,72	1,76	-0,77
TXNRD1	thioredoxin reductase 1	-0.26	0,69	1,07	1,71	-1,52
UBA7	ubiquitin-like modifier activating enzyme 7	-0.91	1,09	0,66	-0,13	-0,82
UBD	ubiquitin D	-0.39	-0,26	-0,74	-0,29	3,53
UBE2C	ubiquitin-conjugating enzyme E2C	0.32	-0,35	0,03	-0,39	2,32
UBE2L6	ubiquitin-conjugating enzyme E2L 6	0.66	1,75	1,90	0,43	-3,32
UIMC1	ubiquitin interaction motif containing 1	0.18	0,49	-2,16	-0,20	-0,20
UPK3B	uroplakin 3B	-0.26	-0,75	-0,87	-0,71	2,02
USP18	ubiquitin specific peptidase 18	0.23	1,04	0,94	0,44	-3,21
UTRN	Utrophin	-0.23	-0,02	0,04	0,19	2,11
VEGFA	vascular endothelial growth factor A	-0.23	0,49	1,30	0,37	-3,39
WARS	tryptophanyl-tRNA synthetase	0.53	1,57	1,14	1,75	-3,93
WNT10A	wingless-type MMTV integration site family, member 10A	0.01	-0,99	-1,04	-0,72	2,07
WWOX	WW domain containing oxidoreductase	0.35	-0,70	0,03	-0,19	1,78
XPOT	exportin	0.57	0,35	0,57	0,59	-2,30
YARS	tyrosyl-tRNA synthetase	0.02	-0,31	0,32	0,28	-2,03
ZC3HAV1	zinc finger CCCH-type, antiviral 1	-0.07	0,33	0,32	0,19	-1,83
ZFP36	zinc finger protein 36, C3H type	-0.45	0,59	0,43	0,94	-1,23
ZNF331	zinc finger protein 331	-0.21	-0,73	-0,75	-0,36	2,08
ZNF587	zinc finger protein 587	0.13	0,31	-0,25	-0,18	2,02
ZNF823	zinc finger protein 823	0.93	-0,73	-1,87	-0,70	2,03
ZNFX1	zinc finger, NFX1-type containing 1	0.07	1,44	1,45	3,55	-3,07
ZWINT	ZW10 interactor	-0.65	-0,10	0,19	0,17	2,27